ISTANBUL TECHNICAL UNIVERSITY ★ GRADUATE SCHOOL OF SCIENCE ENGINEERING AND TECHNOLOGY

PVDF-BASED NANOFIBROUS MEMBRANES FOR ENVIRONMENTAL AND ENERGY APPLICATIONS

M.Sc. THESIS

ADEL AL RAI

Department of Mechanical Engineering

Material and Manufacturing Program

June 2019

ISTANBUL TECHNICAL UNIVERSITY ★ GRADUATE SCHOOL OF SCIENCE ENGINEERING AND TECHNOLOGY

PVDF-BASED NANOFIBROUS MEMBRANES FOR ENVIRONMENTAL AND ENERGY APPLICATIONS

M.Sc. THESIS

ADEL AL RAI
(503161302)

Department of Mechanical and Engineering

Material and Manufacturing Program

Thesis Advisor: Prof. Dr. Şafak YILMAZ

JUNE 2019

ISTANBUL TEKNİK ÜNİVERSİTESİ ★ FEN BİLİMLERİ ENSTİTÜSÜ

PVDF-BASED NANOFIBROUS MEMBRANES FOR ENVIRONMENTAL AND ENERGY APPLICATIONS

YÜKSEK LİSANS TEZİ

ADEL AL RAI
(503161302)

Makina Mühendisliği Anabilim Dalı

Malzeme ve İmalat Programı

Tez Danışmanı: Prof. Dr. Şafak YILMAZ

HAZİRAN 2019

Adel AL Rai, a M.Sc. student of İTU Graduate School of Science Engineering and Technology student ID 503161302, successfully defended the thesis entitled "PVDF-BASED NANO-FIBROUS MEMBRANES FOR ENVIRONMENTAL AND ENERGY APPLICATIONS", which he prepared after fulfilling the requirements specified in the associated legislations, before the jury whose signatures are below.

Thesis Advisor :	**Prof. Dr. Safak Yilmaz** Istanbul Technical University	.....
Jury Members :	**Associate Prof. Dr. Ali Kilic** Istanbul Technical University	.....
	Assistant Prof. Dr. Sunal Ahmet Parasız Sakarya University	.....

Date of Submission : 03 May 2019
Date of Defense : 11 June 2019

To my family,

FOREWORD

I would like to thank my supervisor Prof. Dr. Safak Yilmaz for his supervision, comments, help, kindness, and support. Without his full support from beginning to end, I would not be able to deliver this work today.
I like to express my deepest appreciation for Prof. Dr. Ali Demir for his kindness, encouragement, and support. I thank associate Prof. Dr. Ali Kilic for his support. I thank a Ph.D. candidate Elena Stojanovska for taking the time to help me conduct some experiments and comments and monitor my work. From the bottom of my heart, I thank all TEMAG current and old members of whom I learned plenty and have been a great support as colleagues and friends.
I also thank my good friend Arda Cakiroglu for his ultimate support all the time.
Even though my family is more than a thousand kilometer away, they have always been with me with their thoughts and ultimate love. For that and everything else, I dedicate this humble thesis for them, my family.

June 2019

ADEL AL RAI
(Mechanical Engineer)

TABLE OF CONTENT

Page

ABBREVIATIONS

AFD : Average Fiber Diameter
ACA : Average Contact Angle
BuOH : N-Butanol
CB : Centrifugal Spinning
DMF : Dimethylformamide
ESBS : Electrically-Assisted Solution Blow Spinning
ES : Electrospining
GSM : Gram Per Square Meter
IPA : Isopropyl Alcohol
LIB : Lithium-Ion Battery
$LiPF_6$: Lithium Hexafluorophosphate
MD : Machine Direction
nm : Nanometer
NP : Nano Particle
NTD : Nozzle-To-Collector Distance
PA6 : Polyamide, 6
PAN : Polyacrylonitrile
PE : Polyethylene
PI : Polyimide
PM : Particulate Matter
PMMA : Poly(methyl methacrylate)
PP : Polypropylene
PVDF : Poly(vinylidene Fluoride)
SBS : Solution Blow Spinning
SEM : Scanning Electron Microscopy
TD : Transverse Direction
TS : Touch Spinning
um : Micrometer

SYMBOLS

A	**:** Area
C	**:** Concentration
FR	**:** Flow rate
kV	**:** Kilo voltage
L	**:** Length
M	**:** Mass
P	**:** Penetration
p	**:** Pressure drop
Q	**:** Quality factor
t	**:** Time
W	**:** Weight
ρ	**:** Density

LIST OF TABLES

Page

LIST OF FIGURES

Page

PVDF-BASED NANOFIBROUS MEMBRANES FOR ENVIRONMENTAL AND ENERGY APPLICATIONS

SUMMARY

In this thesis, PVDF-based and PVDF/blend-based nanofibrous membranes were developed and characterized for environmental energy applications. Those membranes were manufactured using a technique called Electrically-assisted Solution Blow Spinning to meet the development of Aerosol Air Filtration and Separator for Lithium-ion Battery applications.

First, Eclectically-assisted Solution Blow Spinning is simply nanofiber production method, which uses, as the name suggests, electric potential and pressurized air for fiber formation. This technique brings together the features of Electrospinning and Solution Blow Spinning in one setup. With this technique, one can expect to have more control over the end product and production at a high rate.

PVDF-based nanofibrous membranes were developed and characterized for aerosol air filtration application. In this work, a parametric approach was adopted in which solution concentration and electric voltage parameters were varied, and the rest of the parameters were kept constant. Solution rheology, surface morphology, pore size distribution, and filtration properties before and after charge elimination were evaluated and investigated. Results show that solution concentration and electric voltage affect average fiber diameter and average pore size dramatically and, consequently, filtration efficiency. Additionally, electric voltage facilitates the bombarding of electrostatic charges that have resulted in obvious electret properties and led to increase in the filtration efficiency of those membranes.

Separately, PVDF/modacrylic/SiO_2-based nanofibrous membranes were developed and characterized as a separator in Lithium-ion battery application. The aim is to develop a separator for high safety and performance lithium-ion battery. In other words, the aim of this work is to develop a nanofibrous membrane of high porosity, high electrolyte uptake, and thermally and mechanically stable. A systematic approach was adopted in which all the system, process, and material parameters were kept constant except for blend ratios. First, PVDF/modacrylic blend weight ratios of 100:0, 75:25, 50:50, and 25:75 at a constant solution concentration of 13 wt.% were spun. The different samples were characterized for their porosity, electrolyte uptake, dimensional and thermal stabilities, ionic conductivity, and mechanical properties. Resells show a significant improvement compared with the results of the available commercial separators. The addition of Modacrylic enhanced the porosity, electrolyte uptake, and thermal and mechanical stabilities. These enhancements would promote high safety and performance lithium-ion battery. Moreover, after the addition of hydrophilic fumed SiO_2 nanoparticles at different concentrations to PVDF/modacrylic-based membrane (PVDF/modacrylic of a weight ratio of 50:50 wt.%), some of the separator properties were further enhanced. Results show the addition of those nanoparticles, at small fractions (0.1 and 1 wt.%) increase porosity,

and thus, higher electrolyte uptake has achieved. Interestingly, at only a weight fraction of 0.1 wt.% dimensional stability of the membranes was enhanced, which promotes high safety lithium-ion batteries. Ionic conductivity results show PVDF/modacrylic-based nanofibrous membrane has higher ionic conductivity than commercial PP separators due to higher porosity and high electrolyte uptake. Furthermore, PVDF/modacrylic-based nanofibrous membrane adds a flame-retarding property to the membrane and enhances mechanical properties compared with polyacrylonitrile-based membrane. Generally, the addition of modacrylic and SiO_2 nanoparticles provide a solution to safety issues in lithium-ion battery and promote them as a substitution for brittle and somewhat flammable PP and polyacrylonitrile-based membranes.

ÇEVRE VE ENERJİ UYGULAMALARI İÇİN PVDF NANOLİF YAPILI PVDF MEMBRANLAR

ÖZET

Bu tezde, çevreci enerji üretim yöntemlerine yönelik PVDF bazlı ve PVDF/karışım bazlı nanofiber membranların tasarımı yapılıp bu membranlar üretilmiş ve üretilen bu malzemelerin karakterizasyon analizleri yapılmıştır. Bu membranlar yeni geliştirilen Aerosol Hava Filtrasyonu ve Lityum-İon Bataryaları alanlarında kullanıma yönelik olarak özel ve özgün bir Elektrik-destekli Çözeltiden Üfleme ile Eğirme yöntemi ile üretilmiştir.

İlk olarak kullanılan Elektrik-destekli Çözeltiden Üfleme ile Eğirme yöntemini kısaca açıklamak gerekirse, bu yöntem geleneksel Elektro-eğirme ve Çözeltiden Üfleme adlı iki sık kullanılan ve oldukça olgunlaşmış iki yöntemin birleştirilmesi ile oluşmuş bir üretim şeklidir. İki yöntemin birleştirilmesi ile Elektro-eğirme ve Çözeltiden Üfleme yöntemlerinin birbirinden farklı olan avantajlı noktalarının biraraya getirildiği ve bu iki yöntemin dezavantajlarının oratk bir sinerji ile aynı anda minimize edildiği bir üretim yöntemi oluşturulmaya çalışılmaktadır. Bu şekilde hem eğirme sonucunda ortaya çıkan son ürünün özelliklerini daha iyi kontrol edilmesi, hem de üretim hızının arttırılması amaçlanmaktadır.

Ek olarak, sistem büyük ölçüde nanofiber membran üretme maliyetini düşürebilir. Bu büyük bir üretim oranını destekleyerek mümkündür.

Kısacası bu çalışma, aerosol filtrasyonu ve lityum-iyon pil uygulamaları için düşük maliyetle yüksek kaliteli membranların geliştirilmesinde önemli bir anlayış sağlar. Birincisi, bu çalışma elektret aerosol filtre ortamı geliştirmek ve ikincisi de güvenlik ve yüksek performanslı lityum iyon pil için ayırıcı olarak nano lifli bir zar geliştirmek ile ilgilidir.

PVDF-bazlı nanofiber membranlar Aerosol hava filtrasyonu alanında kullanıma uygun şekilde üretilmişlerdir. Bu çalışmada, bir değişken haricinde tüm diğer değişkenlerin sabit tutulduğu ve bu değişkenin farklı değerlerinde aynı deneyin tekrarlanıp, üretimde ortaya çıkan her bir numunenin karakterizasyon analizlerinin yapıldığı ve her bir değişken için tekrarlanan adımlar sonrasında tüm sonuçların ayrı ayrı karşılaştırılmasının yapıldığı parametrik bir çalışma yapılmıştır. Bu parametrik çalışmada değiştirilen iki parametre çözelti derişikliği ve elektrik voltajıdır; diğer parametreler sabit tutulmuştur.

Çözelti reolojisi, yüzey morfolojisi, filtrasyon etkinliği testleri, elektrik yüklerinin yok edilmesinden önce ve sonra iki kere yapılarak sonuçlar gözlemlenmiş ve ölçümlenmiş, bu özellikler üzerinden üretilen membranın performansı etüt edilmiştir. Sonuçlar, çözelti derişikliği ve elektrik voltajı parametrelerinin fiber çapı ve ortalama gözenek çapını, dolayısıyla da filtrasyon etkinliğini büyük ölçüde etkilediğini göstermiştir.

Ayrıca elekrik voltajının varlığı elyaf tanelerinin elektrik yükleriyle bombalanmasına izin vererek membranın elektriksel olarak polarize olmasına olanak vermekte, bu da filtrasyon etkinliğinin daha da güçlenmesine olanak sağlamaktadır.

Aerosol elektret filtre ortamının tek adımda geliştirilmesi mümkündür. Bu geliştirilen malzemelerin filtrasyon özellikleri, literatürdeki yeni geliştirilen membranlarla karşılaştırıldığında nispeten düşük bir basınç düşüşünde yüksek filtrasyon verimlerine sahiptir.

İkinci grup deneylerde PVDF / modakrilik-SiO_2 bazlı nanofiber membranlar üretilmiş ve üretilen bu membranların lityum-iyon bataryalarında ayırıcı olarak kullanımına yönelik karakterizasyon analizleri yapılmıştır. Bir önceki deney grubunda yapılanın aksine bu gruptaki deneylerde iki katlı sistematik bir yöntem kullanılmış ve sistem, proses ve malzeme parametreleri sabit tutularak sadece karışım oranları değiştirilerek bu farklı değerler için deneyler yapılmıştır.

İlk olarak tüm karışım içinde sabit bir oran olarak %13 oranındaki PVDF / modakrilik karışımında PVDF ve Modakrilik ikilisi dört farklı oranda karıştırılarak deneyler yapılmıştır. Bu dört farklı numune karakterizasyon analizlerine tabi tutulmuş ve porozite, elektrolit emilimi, iyonik iletim ve boyutsal kararlılık testlerine sokulmuştur.

Daha bu noktada analiz sonuçları, halihazırda üretilen ve satılan ticari ayırıcılara nazaran büyük ve umut verici gelişim ve iyileştirme göstermiştir. Ancak bu noktada durulmayıp elde edilen ayırıcıların işlevselliğinin arttırılması amacıyla bir adım daha atılmıştır. Bir önceki sonuçlar incelenerek, numunelerin içinden en umut verici olan PVDF/Modakrilik'in %50:50 karışımı yüksek boyutsal kararlılık ve elektrolit emilimi gösterdiği için bir sonraki adım için seçilmiştir. Bu adımda hidrofilik SiO_2 nanopartiküllerinin polimere olan ağırlık oranında değişikliğe gidilmiştir.

Sonuçlar ağırlıkça % 0.1 ile % 1 gibi çok ufak oranlarda bile polimere katılan bu nanopartiküllerin nanofiberin porozitesini arttırdığını ve dolayısıyla elektrolit emilimini yükselttiğini göstermiştir. Boyutsal kararlılığa gelindiğinde ise polimerin içerisine bu arallığın alt limitinde nanopartiküllerin katılımının bile (ağırlıkça % 0.1) 140º C'de ayırıcının boyutsal kararlılığını arttırdığı ve böylece yüksek oranda güvenli lityum iyon bataryalarının üretimine olanak sağladığı görülmüştür.

İyonik iletkenlik sonuçları, PVDF / modakrilik bazlı nano lifli membranın, yüksek porozite ve yüksek elektrolit alımına bağlı olarak ticari PP ayırıcılardan daha yüksek iyonik iletkenliğe sahip olduğunu göstermektedir. Ayrıca, bu iyonik iletkenlik, SiO_2 nanopartiküllerinin eklenmesinden sonra daha da geliştirilmiştir.

Ayrıca, PVDF / modakrilik bazlı nano lifli membran, membrana bir alev geciktirici özellik ekler ve poliakrilonitril bazlı membran ile karşılaştırıldığında mekanik özellikleri geliştirir. Genel olarak, modakrilik ve Si02 nanoparçacıklarının eklenmesi, lityum-iyon bataryadaki güvenlik sorunlarına bir çözüm sunar ve bunları, kırılgan ve biraz yanıcı PP ve poliakrilonitril bazlı membranların bir ikame olarak destekler.

Modakrilik ve SiO2 içeriğinin, Lityum-iyon bataryadaki bir ayırıcı için mükemmel bir temel malzeme olduğu gösterilmiştir.

Sonuçta, bu çalışma hava filtrasyonu ve enerji uygulamaları için fonksiyonel membranlar geliştirmiştitir.

1. INTRODUCTION

1.1 Purpose of Thesis

This thesis aims to study and develop high functional nanofibrous membrane for environmental and energy applications. For that purpose, electrically-assisted solution blown PVDF-based and co-PVDF/modacrylic/SiO_2-based nanofibrous membranes were developed and characterized for use as aerosol filter membrane and separator in LIB.

On one hand, it is hypothesized that electrically-assisted solution blown PVDF-based nanofibrous membrane to provide enhanced filtration properties by maybe reducing average fiber diameter and pore size and enhancing its electret property.

On the other hand, taking into account that ESBS may promote lower pore size and enhance morphology, ESBS nanofibrous membranes may be able to enhance the separators role in LIB and provide higher porosity membranes capable of increasing uptake values and, thus, ionic conductivity compared with the conventional available commercial membrane. Additionally, PVDF/modacrylic blend may provide high affinity to LIB electrolytes and better thermal stability than the available commercial separators. Moreover, the addition of inorganic hydrophilic SiO_2 NPs into the PVDF/modacrylic nanofibrous membrane may even further enhance porosity, wettability, and other properties.

1.2 Literature Review

1.2.1 Nanofibrous membrane

1.2.1.1 Properties of nanofibrous membrane

A nanofibrous membrane is a thin nanoporous layer made of oriented or randomly oriented interconnected nanofibers that possess high surface area to volume ratio. The

fiber diameter is smaller than 1 µm. These nanofibrous membranes are of great interest in many applications, such as separator in Lithium-ion battery and aerosol filter membrane [1].

Chemical and physical properties functions define the end use of these membranes. Some of these properties (chemical, thermal, and mechanical properties, degradability, porosity, fiber and pore size distribution, average diameter, hydrophobicity, permeability, handleability) are modified based on the final use of the membrane.

1.2.1.2 Base material of nanofibrous membrane

Mainly the selection of the materials can be classified into two categories: polymeric and non- polymeric materials. Polymeric materials include, but not limited to, Polyvinylidene fluoride (PVDF), polyacrylonitrile (PAN), thermoplastic polyurethane (TPU), polyamide 6 (PA6) and polyamide 6,6 (PA6,6), polyvinyl alcohol (PVA), Polytetrafluoroethylene (PTFE) and many other [2–4]. On the other hand, the non-polymeric materials are made up of ceramics such as TiO_2 and SiO_2 [5,6]. Hybrid material such as the incorporation of nanoparticles into or onto the fibers has been developed as well [7,8].

1.2.1.3 Production methods of nanofibrous membrane

Bottom-up. Bottom-up refers to the case at which molecules come together for self-assembly at the molecular level. Under this category falls self-assembled nanofiber. The morphology of these fibers can be controlled by controlling the effective parameters, which are concentration, solvent, and temperature. The fiber can be as small as 10 nm in diameter; however, the length is rather limited. One of the main drawbacks is the produced fibers are difficult to be obtained as a freestanding membrane, which a supporting scaffold is required [9]. Nonetheless, some limited attempts have been made in order to produce self-assembled nanofibrous membrane. In one study, self-assembled Benzenetrisamide nanofibers have been produced [10]. The fiber diameter distribution a has high homogeneity. In addition, they show that with this method the mechanical properties can be tuned. In a separate study, more promising self-assembly fiber formation has been realized [11]. The method is complicated and consists of multi-steps. In short, amphiphilic N-amidated 4-

aminobenzoic acid sodium salts (with a polar head and a hydrophobic tail) goes under gelation after self-assembly and being mixed with sodium hydroxide solution and poured into a mold and left to cool down. The sample was removed and rinsed from the excess solution and a freestanding hollow nanofibrous membrane was produced as Figure 1.1 shows.

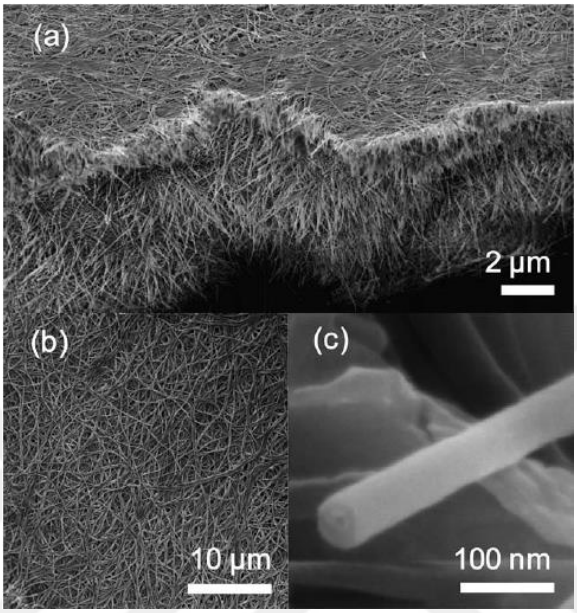

Figure 1.1: SEM images of self-assembled freestanding hollow nanofibrous membrane a) cross section, b) top view, and c) individual hollow fiber [11].

All and all, bottom-up provides a unique way to produce self-assembly nanofibrous membrane but suffers from the limitation on material selection and the possibility of scaling up to meet industrial demands.

Top-down. In the top-down method, the material is processed into the final required shape. The final shape depends upon the parameters of the utilized method. In this literature review, only the most unconventional and promising methods are presented and discussed.

Touch spinning (TS). It is a very simple and straightforward method. A glass rod is attached vertically to the outer edge of circular disk opposing a dangled polymer droplet from a tip of a needle connected to a syringe pump. When the disk starts to rotate at high speeds, the tip of the rod touches the polymer solution droplet and draws it away from the needle, the solvent starts to evaporate, and fibers are formed as Figure 1.2 shows. The system is capable of using polymer melt instead of polymer solution;

however, the melt cools down while it is drawn away from the needle. Moreover, a frame could be used at the tip of the rod to produce different configurations of 3D interconnected nanofibers. The morphology can be controlled with the change of the following parameters: solution concentration and disk rotating speed. A freestanding nanofibrous membrane is possible with the use of multiple rods (brushes). Though the system is scalable, the polymer melt or the solution are laid under the rotating disk in an open environment, which may be hazardous to the environment and human beings alike due to the flammability of some of the used materials and the negative effect on health [12].

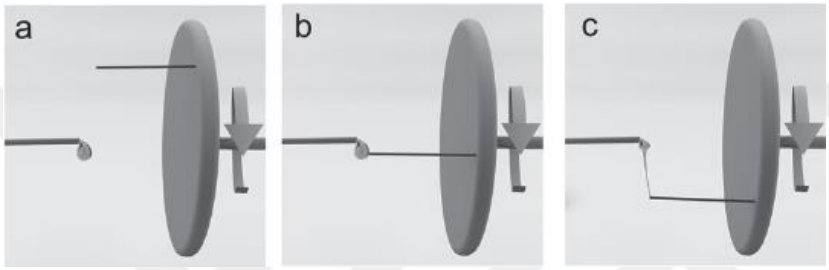

Figure 1.2: Touch spinning method a) before initiation, b) touching and c) fiber attenuation [12].

Electrospinning (ES). Utilizes a conductive polymer solution fed from a syringe pump through a gauge needle and connected to a high voltage power supply, while on the other end, a collector on which the produced fibers are collected is grounded. The mechanism is to attenuate fibers from the tip of a solution droplet using electric forces as Figure 1.3 shows. This occurs when charges accumulate at the tip of the needle and then due to the applied electric field and Columbia forces (after a critical voltage has surpassed the surface tension force of the solution droplet) a Tylor cone is formed. Now, from the end of this cone, a straight small region of polymer jet takes a place, then, whipping and a chaos regions dominate the rest of the journey of the attenuated fiber [13]. The system has attracted many researchers over the last twenty years or so to experiment and explore its potential [13–15]. The produced fibers are of high quality; however, the low production rate (< 10 $g.h^{-1}$) hinders its transition into the industry [16]. Some attempts were conducted to scale up the process, however, they faced some critical issues such as losing the power of electric filed in the center of a packed spinneret system and dripping instead of fiber formation was reported [17].

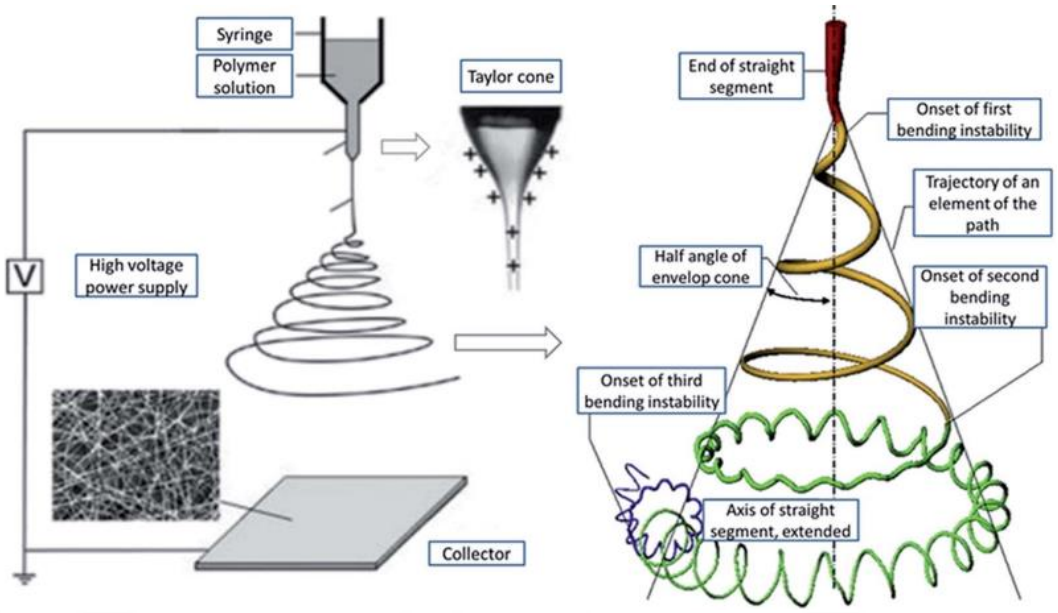

Figure 1.3: Schematic of electrospinning production method and the formation of Tylor cone [18].

Centrifugal spinning. According to Figure 1.4 below, the system consists of two spinnerets attached to a head to which is connected with a rotating motor. After the solution is fed through the spinnerets and the head reaches a critical rotational speed, fiber formation occurs. In spite of the ease of implementing the system, it is capable of high production of around 50 $g.h^{-1}$, which is at least 5 times the production rate of electrospinning. The intrinsic solution and process parameters can be controlled to enhance and modify the morphology of the nanofibrous membrane [19]. The practicality of scaling up the system with high-speed motor(s) may not be very attractive in point of view of industry.

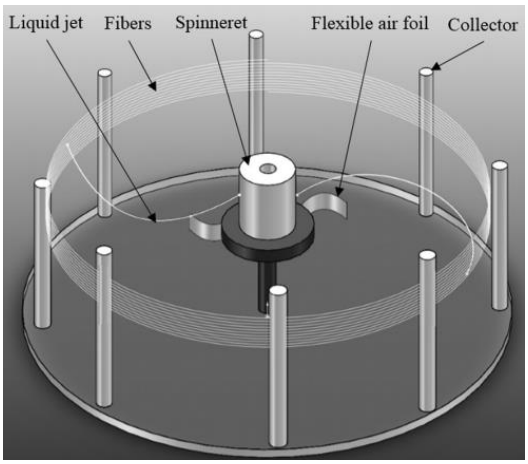

Figure 1.4: Schematic of the centrifugal spinning production method [19].

Solution blow spinning (SBS). A concentric nozzle facilitates polymer solution flow rate and pressurized gas to attenuate fibers from the tip of a spinneret. At the other end of the nozzle, a collector, with a powerful exhaust or a blower, can be used to collect the fibers. In this method, fibers are attenuated from a droplet of a polymer solution as a result of aerodynamic forces and bending perturbations [20–22]. A typical set up of the system is shown in Figure 1.5. The productivity of the system may reach up to 20 times higher in productivity compared with electrospinning [23]. In one study, they show that the system is capable of producing nanofibers with packed nozzles in a single die geometry [24].

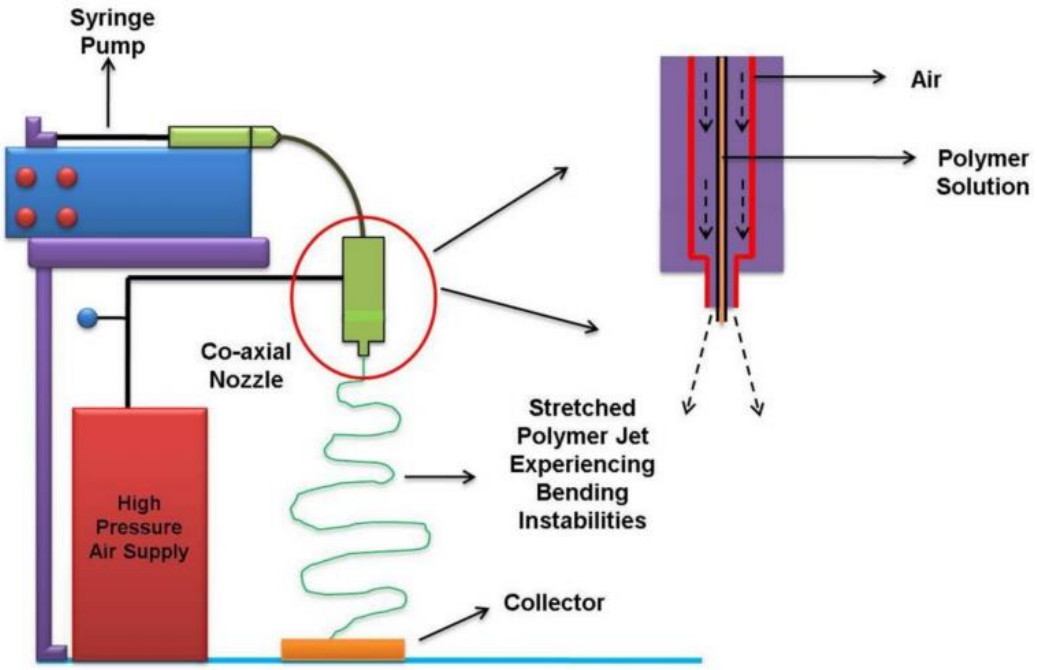

Figure 1.5: Schematic of solution blow spinning production method and its typical concentric nozzle [25].

Electrically-assisted solution blow spinning (ESBS). ESBS has the same principle of a solution blow spinning with the addition of voltage power supply as an additional drawing force as Figure 1.6 shows. This system brings together the high-quality fiber formation from ES and the exceptional high productivity of SBS in one set up that is capable of producing a freestanding nanofibrous membrane. The tip of the nozzle is connected to the electric voltage power supply, while the collector is grounded. The comprised gas reservoir consists of either air or nitrogen gases. A study shows by varying air pressure at a constant electric voltage the fiber morphology and the material

intrinsic properties such as crystallinity of PVDF-based nanofibrous membrane can be enhanced [26]. The system parameters are summarized in Table 1.1 [24,26].

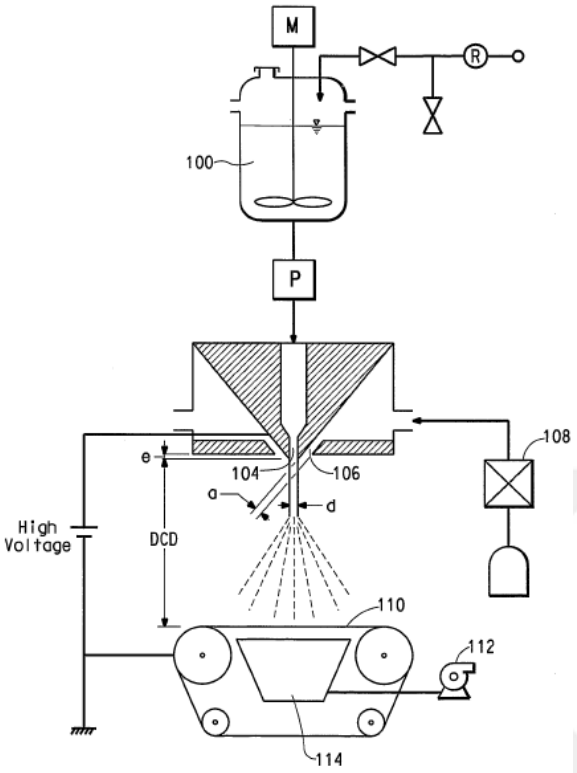

Figure 1.6: Schematic of electrically-assisted solution blow spinning production method [27].

Table 1.1: ESBS parameters [24,26].

Parameter	Assigned name
Material	Viscosity
	Polymer concentration
	Molecular weight
	Surface tension
	Vapor pressure
	Conductivity
Process	Electric voltage
	Air pressure
	Nozzle collector distance
	Flow rate
	Revolution
	Stroke motion
System	Nozzle diameter
	Air nozzle diameter
	Polarity
Ambient	Temperature
	Humidity
	Atmospheric pressure

In conclusion, top-down systems show their superiority over bottom-up systems; however, not all systems in top-down category are the same. ES has shown its capability of producing high quality and very fine nanofibers but at the same time, it lacks the appropriate capability of high production rate. ES and TS are maybe more appropriate for lab scale. On the other hand, CF and SBS provide high production rate systems but perhaps with less quality than ES. ESBS combines the best quality of ES and SBS in on set, which makes it more effective.

1.2.2 Nanofibrous membrane use as an aerosol filter

1.2.2.1 Aerosol filtration

One of the most concerns humanity faces today are environmental issues and air pollution is on the top of this long list. Particulate matter (PM) air pollution is the results of many factors, e.g. industry abnormal emissions, fossil and fuel-based transportation [28]. According to the Wrold Heath Orgnization, air pollution leads to around 7 million deaths each year worldwide. That has led to high efficiency filter membrane to receive great attention recently [28–30]. One of the most promising filter membranes is fibrous membrane and especially nanofibrous membrane. Glass fiber is one of the oldest and most used material as filter media [31].

1.2.2.2 Aerosol filtration theory and mechanism

There are four different capturing mechanisms in air filtration as Figure 1.7 shows.

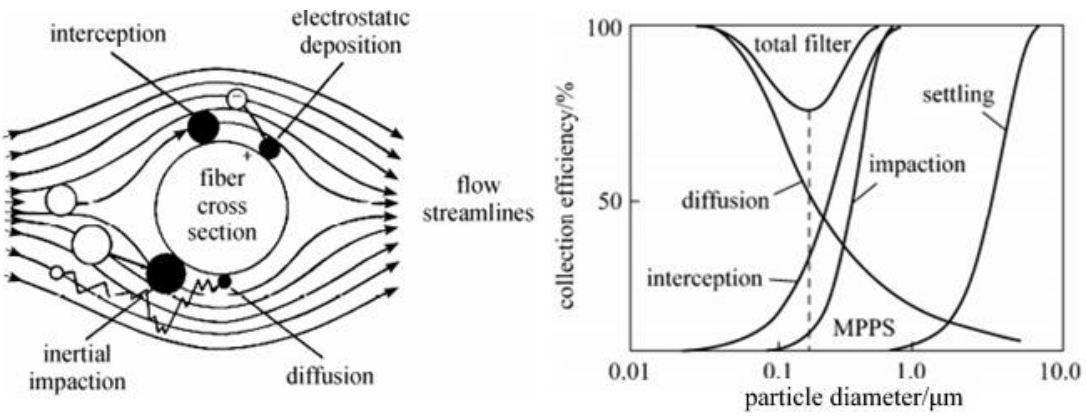

Figure 1.7: Schematic of filtration mechanisms and their filtration efficiency [32].

Inertial Impaction Mechanism. This occurs to the particles that have high inertia, which allows them to shift from the main air streamlines [30].

Interception mechanism. This occurs when the particle does not have enough inertia to break from the streamline but continues with the flow until its diameter touches the diameter of the fiber. This occurs when the distance between the particle and the diameter of the fiber is equal or smaller than the particle diameter [30].

Diffusion Mechanism. This happens to the very small particles (< 0.1 µm) at which they have random movement inside the streamline. This can be explained with the kinetic theory of gases. Basically, gaseous molecules are separated from each other and do not follow the streamline because they keep colliding with each other, which results in random and chaotic paths. Such motion defined as Brownian motion [33,34].

Electrostatic Effect Mechanism. This occurs when the particle or the fiber has electric or electrostatic charges and as a result, the particle is attracted or pulled toward the fiber. This also attracts uncharged particles. These particles get polarized due to the high electric field exerted from the charged fibers, which, then, they are attracted toward the charged fibers [33].

1.2.2.3 Methods to increase capturing efficiency

Nanofibers. Utilizing nanofibers is capable of increasing capturing efficiency and life span of the filter membrane. That is possible because they benefit from a phenomenon called slip-flow that allows for higher capturing efficiency at lower pressure drop compared with micro size fibers [34]. In addition, they have high surface area to volume ratio, which allows one to use higher number of fibers at low basis weight. [35,36].

Electret filter. This is possible with the incorporation of charged particles or polarization of the used fibers [37]. Studies have shown that this is possible with utilizing polymeric material with high dielectric constant with or without the addition of nanosized particles [30,38,39].

1.2.3 Nanofibrous membrane use as a separator in LIB application

This work is devoted to the development of nanofibrous membrane use as separator in Lithium-Ion Battery (LIB) applications. LIB is a rechargeable battery, which consists of three main components: positive (anode) and negative (cathode) electrodes, separator, and electrolyte. Lithium ions travel from the negative electrode to the positive electrode while the battery is discharging and then travel in the opposite direction during charging. A typical electrolyte is composed of lithium ions and facilitates their movement within its liquid form [40]. The separator component plays a crucial role in LIBs: 1) separates the electrodes physically from each other, 2) absorbs and retain electrolyte solution, 3) and provides a medium for ion transportation during charging and recharging cycles as Figure 1.8 shows.

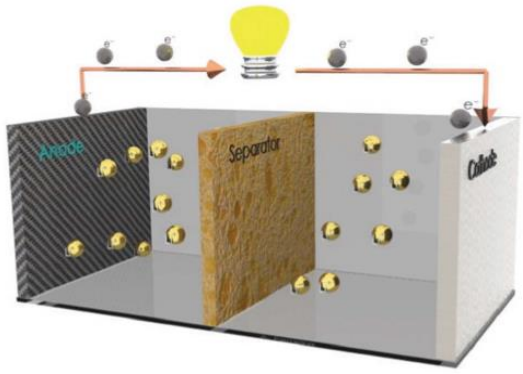

Figure 1.8: Schematic working principle of LIB [41].

The base material of a separator is one of the most important factors that influence its characteristics and performance in LIBs. These characteristics and specifications are:

1) to be chemically and electrochemically stable to withstand the interaction with the electrolyte,

2) to facilitate ionic from and to the electrodes,

3) and, to be stable for a long period of time [42].

Some of the most suited polymeric materials for separators include, but not limited to, poly(methyl methacrylate) (PMMA), polyacrylonitrile (PAN), poly(ethylene) PE, poly(propylene) PP, poly(ethylene oxide) PEO and PVDF and its copolymers [43–50]. Out of the aforementioned materials, PAN and, to a higher extent, copolymer PVDF

(co-PVDF) have been known to their electrochemical stability, mechanical stability, high wettability, and other characteristics in LIB applications [51–54]. In one study, a PVDF/PAN blend membrane was fabricated using phase separation method. The results showed that the higher the content of PAN the higher the dimensional stability of the separator (they can stand shrinkage of about 12% at 160 $^{\circ}$C for one hour) and enhanced the electrolyte uptake compared with commercial separators. Porosity as high as 81% was achieved and the addition of PAN has decreased porosity [55]. In another study, sandwich-type structure co-PVDF/PAN blend nanofibrous membranes were fabricated [56]. Results show these membranes reach high ionic conductivity of about 10^{-3} S.cm^{-1} at room temperature, and higher electrolyte uptake and electrochemical stability than commercial polyethylene separators (PE). The authors conclude that the all different configuration of PAN/co-PVDF based membranes bring together the superiority of each polymer individually in one membrane which makes it superior over PAN or co-PVDF individual membrane. Now, it is worth looking into the drawbacks of PAN and co-PVDF and address them individually. Though PAN has a decent mechanical property and chemical stability, the cyanide group (C≡N) interacts with lithium salts and results into weak interfacial stability, plus PAN suffers from leakage of the electrolyte [57–59]. Now, despite the high electrochemical stability and low crystallinity of co-PVDF, a co-PVDF-based membrane has somewhat low mechanical strength and low thermal stability [60].

The structure and morphology factors (thickness, porosity, and average pore size) are important aspects of separators in LIB. The thickness should not be too thick, in order not to hinder the movement of ions and therefore increases ionic resistivity. And at the same time, It should not be too thin, which otherwise, the electrodes might touch and provoke an electric short circuit that may result into thermal runaway and eventually into the explosion of the battery [61]. Thickness as low as 9 μm is acceptable as long as it has a uniform thickness across the membrane and is easy to manufacture as well [62]. Another morphological factor is porosity. The higher the porosity is the higher the electrolyte uptake and, thus, the higher the ionic conductivity. However, high porosity membrane would suffer from lower mechanical properties [55]. The third morphological aspect is pore size. A uniform pore size distribution is required for better current distribution [63]. Moreover, the pore size should not be too small nor too large so that would not hinder the movement of ions back and forth and would not

let parts of the electrodes go through the separator to the other electrode, respectively [42].

Another critical function of ideal separators is the overall thermal performance. In this regard, dimensional stability falls in this category, which it refers to the separator's ability to withstand elevated temperature and continue to be dimensionally stable, with no changes on it shape such as shrinking, wrinkling, and curling up. Shrinkage of less than 5% after one hour of heating at 90 $^{\circ}$C has been established as an acceptable reference point [62]. The addition of inorganic materials such as SiO_2, Al_2O_3, and AlO_2 into separator membrane in the form of nanoparticles (NPs) have increased the dimensional stability [64–66]. Though the nanofibrous separator studies generally promote that the addition of inorganic NPs that help to boost up the dimensional stability, there are some reports that mention after the addition of NPs the crystallinity decreases and consequently the dimensional stability may be affected negatively [67]. Another thermal function is the shutdown and melting temperatures. The first one refers to the temperature at which the membrane blocks the transportation of the ions by closing up the pores and, thus, decreasing ionic conductivity when the battery undergoes some abnormal situations, e.g. overcharging and short circuit. This shall cause the temperature of the LIB to rise [68]. Therefore, low shutdown temperatures are favorable. While the later, as the name suggests, refers to the melting point of the membrane, at which the separator is expected to retain some of its mechanical property when the battery ia heating up. Unlike shutdown temperature, the separators should somehow have high melting temperature to preserve its mechanical properties during some extreme conditions at elevated temperatures to prevent the disintegration of the separator and the ultimate short circuit between the electrodes that may lead to thermal runaway [61]. That said, having relatively low shutdown temperature and high melting point are two contrastive properties and both are related to the base material. This contrastive issue has been addressed by proposing a sandwich-type structure. On one hand, the middle layer possesses low melting point temperature for which play the role of shutting the pores at low temperature and preventing ionic conductivity. On the other hand, the skin layers possess high melting point temperature, which the separator reserves its mechanical integrity at higher temperature [69]. Results show the sandwich-type structure almost does not shrink under two hours of heating at 180 $^{\circ}$C and the weight loss of PI layer is less than 5% at around 470 $^{\circ}$C for which promotes

the high thermal stability of the skin layers. The reason is attributed to the fact that PVDF and PI have a melting point of about 170 °C and 500 °C, respectively.

Electrolyte wettability, uptake, and retention are crucial requirements for a separator to have. Wettability refers to the quickness of the separator to be wet in LIB, while absorption and retention refer to the ability of the separator to absorb and hold the electrolyte, respectively. In another word, good electrolyte wettability leads to better ionic conductivity [42,62]. These can be enhanced with the addition of inorganic material such as SiO_2, TiO_2, and Al_2O_3 [70–72]. In a study, the addition of hydrophilic fumed SiO_2 NPs into a PAN-based nanofibrous membrane has increased the porosity and, consequently, electrolyte uptake, which resulted in higher ionic conductivity. The results also suggest that the addition of these hydrophilic NPs enhances the stability of the NPs inside the solution due to the increase of zeta potential [74].

The mechanical properties are mainly the tensile strength and puncture strength. Tensile strength should be high enough to withstand the tension during the assembly of the separator. In addition, the elongation should not be too much to avoid the contraction on the other side. On the other hand, puncture strength refers to the ability of the separator to withstand a load applied to a needle to penetrate through. Acceptable puncture strength is necessary to prevent parts of the electrode to travel through the other electrodes to prevent short circuit [61,74].

An important factor to be taken into account is the electrical resistance. This refers to the resistivity of the ions in the separator. An indirect measurement, yet proportional, is the measurement of air permeability, which is defined with Gurley number [62].

Finally yet importantly, the total cost of the separator should not exceed 20% of the total cost of the battery. This urges research to find compatible alternative methods to meet industry demands since current methods are complicated and costly [63,75].

Some basic values that reflect the basic requirements for separators in LIB are summarized in Table 1.2.

Table 1.2: Basic parameters and their requirements of a separator in LIB.

Parameter	Requirement
Thickness (µm)	≤ 25
Porosity (%)	> 40
Pore size (µm)	< 1
Shrinkage (%)	< 5 (at 90 °C for 1 h)
Shutdown temperature (°C)	~ 130
Melting point (°C)	> 150
Wettability	Fast and complete
Tensile strength (%)	≤ 2 (offset at ~ 6.9 MPa)
Young‘s modulus (MPa)	≥ 344
Puncture strength (g/µm)	300/25.4
Gurley number (s μm^{-1})	< 0.025

2. MATERIAL AND METHODS

2.1 Material

co-PVDF (LBG Kaynar) and PVDF (761 Kaynar) and Modacrylic were acquired from Arkema and Aksa, respectively. Hydrophilic SiO_2 nanoparticles with 7 nm in diameter 300 series were bought from Aerosil. Dimethylformamide (Tekkim Kimya, 99.9%) and Acetone (VWR Chemicals, 100%) were used as solvents. n-Butanol used for porosity tests. Isopropanol alcohol (IPA) was used to eliminate electrostatic charges. Lithium hexafluorophosphate (1M LiFP6) in EC:DMC:DEC solvent mixture in 1:1:1 volume ratio and 1% VC additive (Gelon, China) was used as an electrolyte solution. The polymers were dried before use at 60 ºC for at least 18 hours in a vacuum oven and the rest of the materials were used they were received. Polypropylene (PP) commercial separator (Celgrad 2500) used for comparative purpose with the developed separators in the present work.

2.2 Design of Experiment

2.2.1 Nanofibrous membrane for aerosol air filtration

Since one of the aims of this work is to investigate the effect of electric voltage on the filtration efficiency of nanofibrous membranes and another aim is to vary solution concentration to see its effect on filtration efficiency as well, electric voltage and solution concentration parameters were attributed as variable parameters. The rest of the parameters were fixed. Now, based on preliminary experiments, it is suggested that ESBS is stable for a stable production once the polymer jet exiting the nozzle is stable and continuous, and that solely depends on the output of air pressure. As a result, air pressure was set to be constant during all the experiment to ensure that polymer jet was stable. A tricky parameter was the distance between the tip of the nozzle and the collector. The distance was chosen based on the following arguments. First, the largest possible distance that is enough to initiate polymer jet using only electric voltage of 10 kV (or electrospinning at 10 kV) was found to be around 42 cm. Second, the shortest

distance possible that is enough for the polymer jet to evaporate and produce dried fiber was between 25 to 30 cm. From these two arguments, 30 cm as the nozzle to collector distance (NTD) has been chosen. Table 2.1 shows variable and fixed parameters. It should be noted that viscosity, in this work, is solely related to the polymer concentration, which it was neglected as a separated parameter and only solution concentration was taken into account as a parameter. The nozzle was connected to a high electric voltage power supply and the collector was grounded. Two solvents were used Dimethylformamide and Acetone. According to the literature, the addition of acetone (weak solvent of PVDF) to a PVDF based solution increases the solution stability [4,76]. Based on preliminary study, higher than 70:30 ratio of DMF/Acetone the polymer jet evaporates very quickly leaving dried fibers on the tip of the nozzle that leads to complete clogging after a short time.

Table 2.1: Design of experiment for developing nanofibrous membrane for the aerosol air filtration.

Calcification	Parameter	Value
Variable parameters	Polymer concentration (%)	12, 16, & 20%
	Electric voltage (kV)	0, 10, 20, & 30
Fixed parameters	Air pressure (bar)	1.3
	Molecular weight	Moderate
	Solvent ratio	70/30
	Nozzle collector distance (cm)	30
	Flow rate (mL/h)	5
	Revolution (rpm)	280
	Stroke motion ($cm.min^{-1}$)	5
	Nozzle diameter (mm)	0.4
	Air nozzle diameter (mm)	5
	Temperature ($^{\circ}C$)	21(±2)
	Humidity (%)	~30 (±2)
	Surface tension	-
	Conductivity	-
	Vapor pressure	-

2.2.2 Nanofibrous membrane for separators in LIB

All the aforementioned parameters in the previous section are fixed and are shown in Table 2.2. Now, a mixture solution of co-PVDF and Modacrylic with different weight ratios were mixed at a constant polymer concentration of 13 wt.% as Table 2.2 shows. The addition of the NPs was of different weight ratios of 0.1, 1, and 10 wt.% based on the polymer weight ratio.

Table 2.2: Design of experiment for developing nanofibrous membrane for development of separator of LIB.

Calcification	Parameter	Value
Variable parameters	Co-PVDF/Modacrylic (wt.%/wt.%)	100:0, 75:25, 50:50, & 25:75
	Polymer-SiO_2 (wt.%)	0.1, 1, & 10
Fixed parameters	Polymer concentration (%)	13
	Electric voltage (kV)	25
	Air pressure (bar)	2
	Molecular weight (co-PVDF)	Low [*Battery solutions with*
	Molecular weight (Modacrylic)	*Kynar® PVDF*]
	Solvent ratio	High
	Nozzle collector distance (cm)	70:30
	Flow rate (mL/h)	30
	Revolution (rpm)	280
	Stroke motion ($cm.min^{-1}$)	5
	Nozzle diameter (mm)	5
	Air nozzle diameter (mm)	0.4
	Temperature ($^{\circ}C$)	5
	Humidity (%)	21 (±2)
	Surface tension	~30 (±2)
	Conductivity	-
	Vapor pressure	-

2.3 Solution Preparation And Development Of Nanofibrous Membranes

2.3.1 Solution preparation for air filtration membranes

Solutions were prepared by mixing the solvents and then they were added to the polymer powder. For example, a mixture of 70:30 ratio of DMF/Acetone was mixed for about five minutes on a magnetic stirrer at room temperature and then it was added to the polymer powder. The whole mixture was placed on a magnetic stirrer at elevated temperature of 65 $^{\circ}C$ for at least 18 hours.

The samples that were produced for aerosol air filtration purposes were deposited on a nonwoven meltblown substrate on which all the subsequent tests were performed. The filtration efficiency of the used nonwoven was reported as well.

In order to control the gram per square meter (GSM) a theatrical constant of GSM of around 0.8 $g.m^2$ was fixed by fixing time deposition. Time was estimated based on equation (2.3)

$$\text{gsm} = \frac{t.\left(\frac{FR}{60}\right).C}{A} \quad (2.3)$$

where t is time deposition in minute, FR is the solution flow rate in mL.h^{-1}, C is concentration in percent, and A is the area of deposited fibers (0.06 m^2).

It is worth mentioning that it was assumed that there was no loss of the fibers during the process of production. Table 2.3 summarize the time deposition for all the distinct produced samples. The temperature of the used polymer solutions before the production of the nanofibrous membranes was the room temperature.

Table 2.3: Time deposition for all distinct produced samples.

Category	Sample code	Time (min)
Filtration samples	12_a	5
	16_b	4.25
	20_c	3

a, b, and c refer to the sample that was produced with solution concentrations of 12, 16, and 20 wt.%, respectively.

2.3.2 Solution preparation for separator membranes in LIB

The polymer blend solution was prepared by first mixing the corresponding co/PVDF and Modacrylic ratio in one pot and then add the required mixrure of the solvent of 70:30 ratio of DMF/acetone. The whole mixture was mixed vigorously for at least 18 at elevated temperature of 65 $^{\circ}$C.

In case when SiO_2 NPs were used, the required amount of the NPs was added after the complete dissolve of the polymer solution. After vigorous stirring at an elevated temperature of 65 $^{\circ}$C for 2 hours, the mixture was ultrasonicated in a Sonicator bath for 2 hours and was used immediately utilized for a production [77].

The samples that were produced for separators in LIB were deposited on silicone oilpapers, which facilitated the removal of the nanofibrous membrane easily for subsequent tests.

Thickness was controlled by depositing fibers continuously for 30 minutes. Again, it is worth mentioning that it was assumed that there was no loss of the fibers during the process of production. Table 2.4 summarize the time deposition for all distinct produced samples.

Table 2.4: Time deposition for all distinct produced samples.

Category	Sample code	Time (min)
Separator samples	All produced samples	30

The temperature of the used polymer solutions before the production of the nanofibrous membranes was the room temperature. For all the samples that were used for further tests, were heat treated at 100 $^{\circ}$C for 1 hour in a vacuum furnace prior usage to ensure complete solvent removal and to increase their handleability.

3. TOOLS FOR PRODUCTION AND CHARACTERIZATION

3.1 Production Tool

For the production of all the nanofibrous membranes using ESBS, an Electroblowing set up was used. This machine trend trademark was AEROSPINNER Electro Blowing Series bought from Areka. The set up consists of an air pressure regulator connected to a compressed air reservoir, electric voltage, power supply, syringe pump, exhaust, rotating collector, and a mobile shaft for homogenous deposition of the fibers. The rotating collector has a length and a diameter of 30 and 10 cm, respectively, that produces a freestanding nanofibrous membrane of 20 cm × 30 cm. Figure 3.1 shows the digital image of the machine.

Figure 3.1: Electroblowing machine.

On the top of the shaft, a concentric single nozzle was placed. Figure 3.2 shows the 3D drawing of the concentric nozzle. The nozzle facilitates polymer solution feed rate, air output, and a connection to the electric voltage power supply.

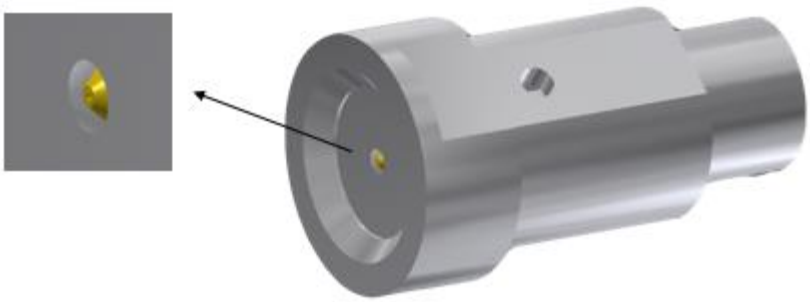

Figure 3.2: 3D technical drawing of the concentric nozzle.

3.2 Rheological Behavior Of The Solutions

A trademark Fungilab rotational viscometer was used to measure the viscosity of the prepared solutions. This test was done by placing the solution underneath a dangled rotating disk, which is attached to a spinning head. After inserting the disk into the solution, the measurement starts. All results were taken after 30 seconds form the initial recorded result on the panel. A digital image of the device is shown in Figure 3.3. The main principle of this viscometer is, in this particular set up, it measures the required torque to rotate a disk that is placed in a fluid as a function of the viscosity. This test was conducted only once.

Figure 3.3: Digital image of a rotational viscometer.

3.3 Surface Morphology Analysis

A trademark Tescan, Vega 3 Scanning Electron Microscopy (SEM) was used to analyze the morphology of the produced samples. The tested samples were cut into small pieces and palladium and gold coated using with a trademark Quorum (model:

SC7620). The fascinating principle behind SEM is depicted in Figure 3.4 and can be described as the following: a heated tungsten electro gun emits a high-energy beam of electrons that accelerate inside an electric field and pass through lenses to generate a focused beam to which hits the surface of the sample inside a vacuumed chamber. Depending on the electron beam energy, secondary, backscattered electrons, and other types of scattering of electrons can be detected, then analyzed, and finally comprehended as a digital image. The average fiber diameter was determined using ImageJ software. At least 100 measurements that distributed over at least four different areas were measured.

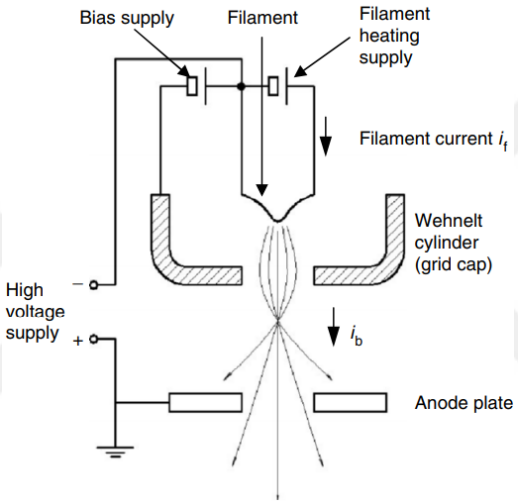

Figure 3.4: Schematic of the working principle of SEM.

3.4 Automated Air Filter Tester

A trademark Certitest automated air filter tester (Model 8130A) was used to measure air filtration efficiency and pressure drop was used as Figure 3.5 shows. After neutralizing NaCl aerosol in the mixing chamber, the NaCl aerosol is sent down to the filter area of 100 cm^2 after which the difference of the concentration of the particles between upstream and downstream is measured. The NaCl aerosol specifications are tabulated in Table 3.1. The filtration efficiency test was done at three different areas across the tested sample.

Figure 3.5: Digital image of automated air filter tester.

Table 3.1: Aerosol specifications.

Specifications of the aerosol	Value
Aerosols	Sodium Chloride
Mass mean diameter	0.26 µm
Count mean diameter	0.07 µm
Standard deviation	<1.83
Concentration	15 to 20 $mg.m^{-3}$

3.5 Vacuum Furnace Treatment

A vacuum furnace was used to heat treat the samples and to measure thermal shrinkage rate at elevated temperatures.

The samples that were used as separators were heat treated only. As spun samples were placed inside the furnace and heated up to 100 $^{\circ}C$, then stayed for 1 hour at that temperature and then left to cool down to room temperature.

For shrinkage test, the samples were cut into small pieces and placed inside the furnace. The temperature gradually increased to 140 $^{\circ}C$ and stayed at that temperature for 2 hours in a vacuum environment. The dimensions before and after heat treatment

were acquired and the thermal shrinkage rate was then calculated using equation (3.5) [78]

$$\text{TSR (\%)} = \frac{L_i - L_f}{L_i} \times 100 \quad (3.5)$$

where L_i and L_f are the initial and final length of the heat-applied separator. This test was measured for both the machine direction (MD) and transverse direction (TD). For accuracy, this test was repeated at least three times.

3.6 Wettability Test

3.6.1 Electrolyte uptake test

The electrolyte solution was a typical lithium hexafluorophosphate ($LiPF_6$) based electrolyte used for R&D LIB studies. This test was done by immersing the tested samples into electrolyte solution for 2 hours in a glove box environment due to the volatility of the solution. The weight of the sample before (dried weight) and after soaking into the solution (wet weight) were measured. The electrolyte uptake was calculated according to the following equation (3.6) [79]

$$\text{EU (\%)} = \frac{W_1 - W_0}{W_0} \times 100 \quad (3.6)$$

where W_0 and W_1 are the weight of the dried and soaked sample.

3.6.2 Contact angle test

This test was done using optical tensiometer (Attension Biolin Scientific) to further confirm the wettability of the produced samples. This test was conducted by dropping a 5 µL droplet of $LiPF_6$ onto a coin size of the tested separator. The measurement setting time was set to 5 seconds, and was triggered once the droplet hit the surface of the sample. The samples were cut into coin battery size of a diameter of 1.4 mm using battery puncher bought from Gelon.

3.7 Porosity Test

This test was done using n-butyl (BuOH) alcohol uptake method. The porosity was determined by measuring the weight of the separator before and after immersing it into BuOH using this equation (3.7) [80]

$$P\ (\%) = \frac{\frac{M_{BuOH}}{\rho_{BuOH}}}{\frac{M_{BuOH}}{\rho_{BuOH}} + \frac{M_m}{\rho_p}} \times 100 \qquad (3.7)$$

where M_{BuOH}, ρ_{BuOH}, M_m and ρ_p, are the mass of the absorbed BuOH, the density of BuOH, mass of the dried nanofibrous membrane, and the density of the polymer, respectively. The densities of polymers, BuOH, and the corresponding densities of polymer for the produced blend samples are summarized in Table 3.2.

Table 3.2: Densities of the polymer and blend polymer of the produced samples as separators in LIB and other materials.

Material	Density ($Kg.m^{-3}$)
BuOH	0.81
co-PVDF	1.78
Modacrylic	1.16
$100:0_a$	1.78
$75:25_a$	0.97
$50:50_a$	1.47
$25:75_a$	0.66

a refers to the produced samples that contain a blend of polymers of different ratios of co-PVDF/modacrylic

3.8 Pore Size Distribution

A bubble point method was used to determine the pore size distribution. Briefly, it measures the needed gas pressure to force an air bubble through the pores. This test was done in the facility of HIFYBER.

3.9 Electrochemical Impedance Spectroscopy

Ionic conductivity test was determined by electrochemical impedance spectroscopy (Potentiostat Garmy ZRA 600+) analysis over a frequency range from 0.1 Hz to 10 kHz at room temperature. A separator sample, was cut into a circular shape with a diameter of 14 mm, was sandwiched between two stainless steel foils and assembled into a coin cell 2032 together with $LiPF_6$ electrolyte. The ionic conductivity was calculated using equation (3.9)

$$\sigma = \frac{t}{R_b A} \tag{3.9}$$

where t and A are thickness and area of the membrane, while R_b is the bulk resistance that is acquired from Nyquist plot of the impedance test.

3.10 Combustion Test

This test was simply conducted by placing the samples close to a source of flame. Digital images and notes were taken during the experiment.

3.11 Mechanical Properties

Tensile test was carried on (Instron 4411) to evaluate mechanical property and flexibility of the membranes. The samples were cut with a length and width of 50 mm, 10 mm, respectively. The test speed rate was of 10 mm/min. Before any measurement was taken, the thickness was measured using a thickness gauge (Mitutoyo 547-401).

4. RESULTS AND DISCUSSION

4.1 Development Of Nanofibrous Membrane As Electret Filter

4.1.1 Rheological behavior of the solutions

Three different concentrations of 12, 16, and 20 wt.% of PVDF solutions were prepared and their viscosities were measured. Results show that the higher the concentration the higher the viscosity. Table 4.1 summarizes the viscosity of the solutions.

Table 4.1: Rheological behavior of PVDF solution of different concentration.

PVDF concentration (%)	Solvent ratio (DMF/Acetone)	Viscosity (mPa.s)
12	70:30	256
16	70:30	1070
20	70:30	3980

4.1.2 Surface morphology analysis

The effect of solution concentration and electric voltage parameters on the morphology of electrically-assisted solution blown nanofibrous membranes was investigated using SEM.

Figure 4.1 shows the SEM images at two different magnifications of the spun membranes prepared using 12 wt.% PVDF concentration produced at 4 different electric voltage outputs. The results illustrate that with the increase of electric voltage, the defects (islands/film-type structures) are minimized. This could be related to the higher electrical voltage that in return results in higher the drawing ratio. This means more drawing forces are acted upon the polymer jet, which attenuates the droplet into finer and finer fibers instead of carrying portions of the solution droplet to the collector. Moreover, the islands are flat because the blown air strikes the membrane directly and flatten these droplets [81]. It is clear that even with no electric voltage applied (0 kV) fibril structure is evident, unlike the case in one study with no electric voltage film-type structure was dominant [81]. The reason for the different findings

may be related to the intrinsic geometry of the different utilized nozzles, assuming the utilized nozzle in this work facilitates smoother fiber formation. In terms of morphology, the same observations were seen with 16% as spun nanofibrous membranes as shown in Figure 4.2. Figure 4.3 shows that 20 wt.% as spun nanofibrous membranes were inferior to the previous nanofibrous membranes produced at different concentrations due to its incapability of producing regular continuous fibril structure. These SEM images show mainly the surface morphology of the nonwoven substrate on which is used to collect the fibers with some dispersed fibril and film-type structures. This may be related to observation was seen during the experiment, which the polymer jet of 20 wt.% solution was in sporadic and discontinuous motion. This may be caused by the high viscous nature of the solution (~4000 mPa.s). That said, results suggest at electric voltage of 30 kV there are more frequent microfibers than at 0 kV. According to the previous discussion, this may be due to the higher drawing ratios applied to the polymer jet. In addition, this may also be due to the increased throughput with high electric voltage [81].

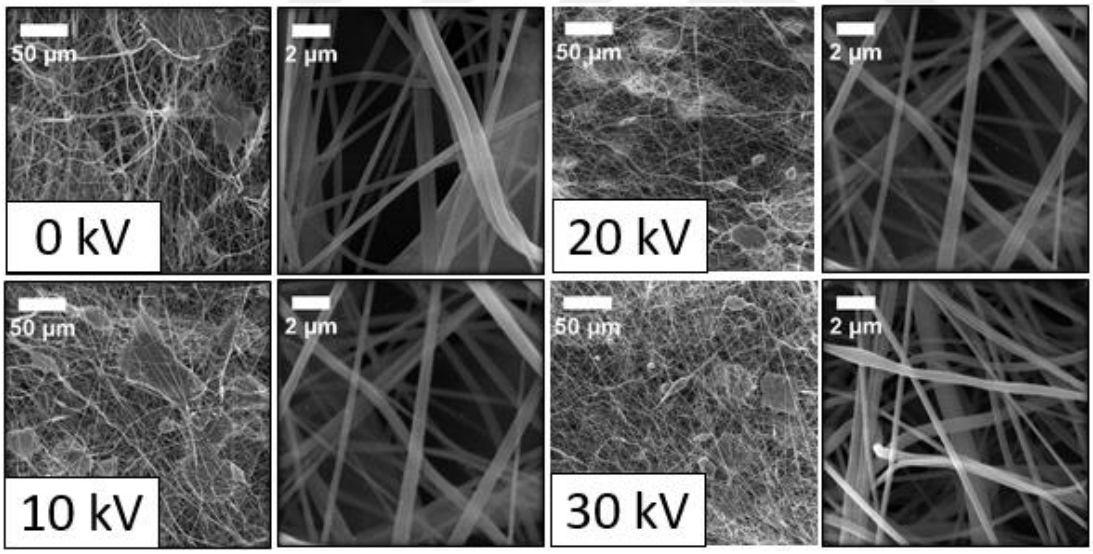

Figure 4.1: SEM images at 500 and 10k magnifications of nanofibrous membrane prepared with 12 wt.% PVDF concentration at: 0 kV, 10 kV, 20 kV, and 30 kV.

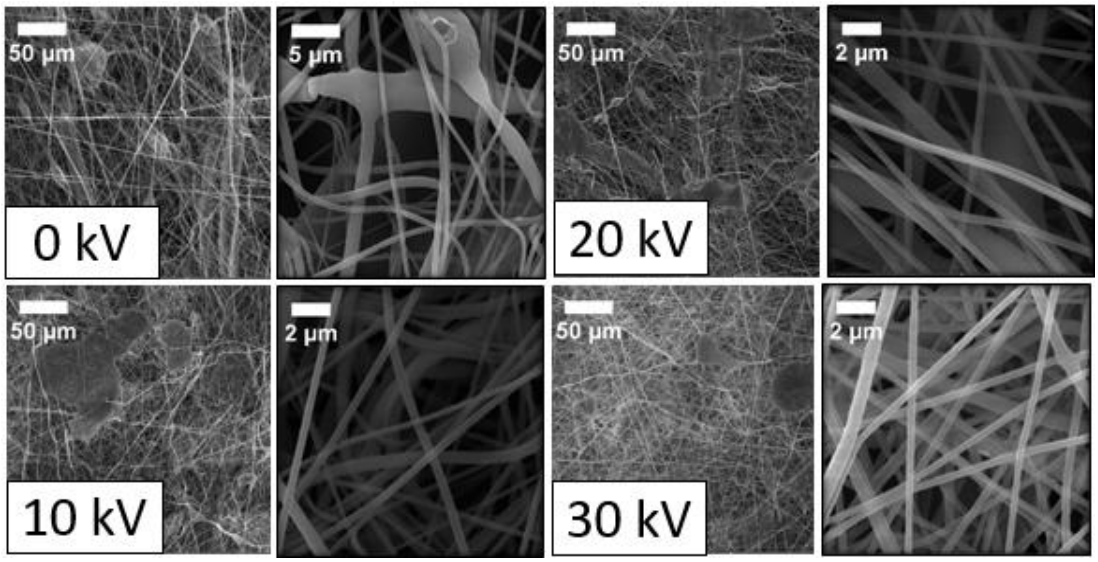

Figure 4.2: SEM images at 500 and 10k magnifications of nanofibrous membrane prepared with 16 wt.% PVDF concentration at: 0 kV, 10 kV, 20 kV, and 30 kV.

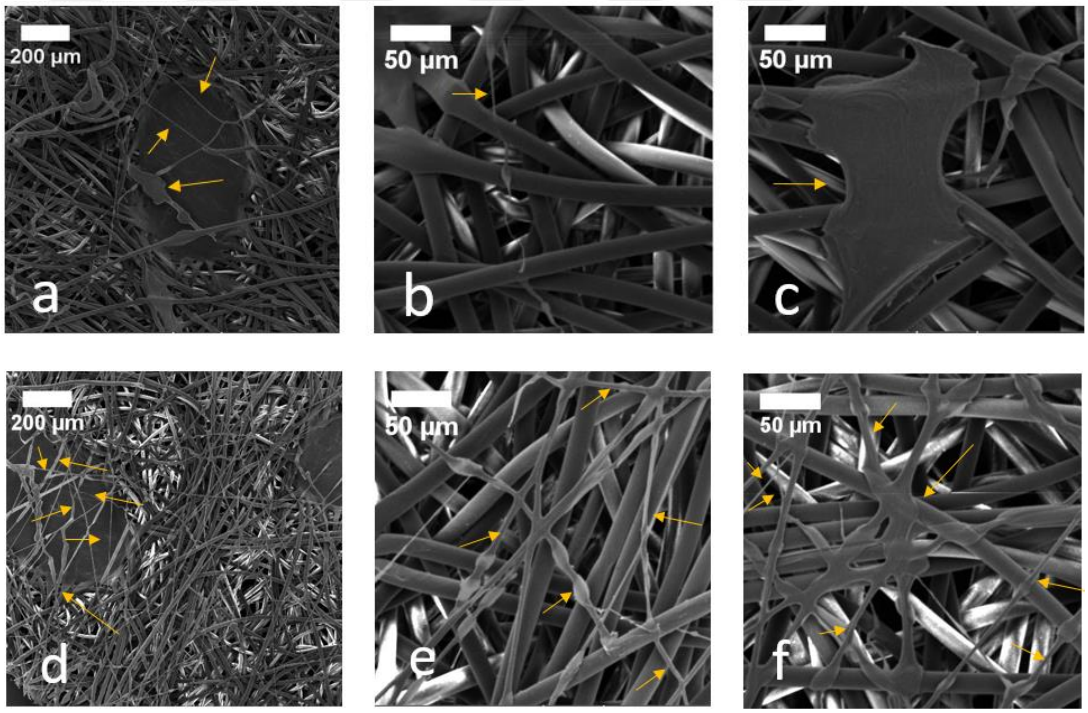

Figure 4.3: SEM images taken at different positions at 100 and 500 magnifications of nanofibrous membrane prepared with 16% PVDF concentration and produced at electrical voltage of: a, b, and c 0 kV, and d, e, and f 30 kV.

Average fiber diameters (AFDs) were calculated using ImageJ software, and AFDs as a function of viscosity are shown in Figure 4.4 and their corresponding statistical results are shown in Table 4.2. Results show that the produced fiber diameters from 16 wt.% concentration have a larger mean than 12 wt.% concentration. This matches the previous finding in the literature, which illustrates AFD is directly related to the

concentration of the polymer solution by power low relationship [82]. Interestingly, the electric voltage had a bit different impact on AFD and fiber distribution depending on the viscosity of the solution. For the as spun nanofibrous membranes produced from 12 wt.% PVDF concentration when electric voltage was 0 kV the AFD was 424 ± 233 nm. While at electric voltage of 10, 20, and 30 kV, the AFDs are in close range but the fiber distribution gets smaller, 347 ± 152, 349 ± 120, and 328 ± 105 nm respectively. This shows that electric voltage has an effect on AFD produced from 12 wt.% solution. Now, for the fibers produced from 16 wt.%, the electric voltage has a similar effect on fiber distribution but perhaps it has a more notable effect on their AFDs. The AFD dropped from 727 ± 366 to 482 ± 184 nm when the electric voltage output increased from 0 to 10 kV. And unlike the membranes produced from 12 wt.% concentration, the AFDs continues to decrees 448 ± 170 and 408 ± 143 nm with the increase of electric voltage at 20 and 30 kV, respectively. It is safe to conclude that the higher the electric voltage the lower the fiber distribution and definitely the lower the AFD at least compared with SBS. In addition, electric voltage may have more impact on AFD that is produced from high viscous solutions.

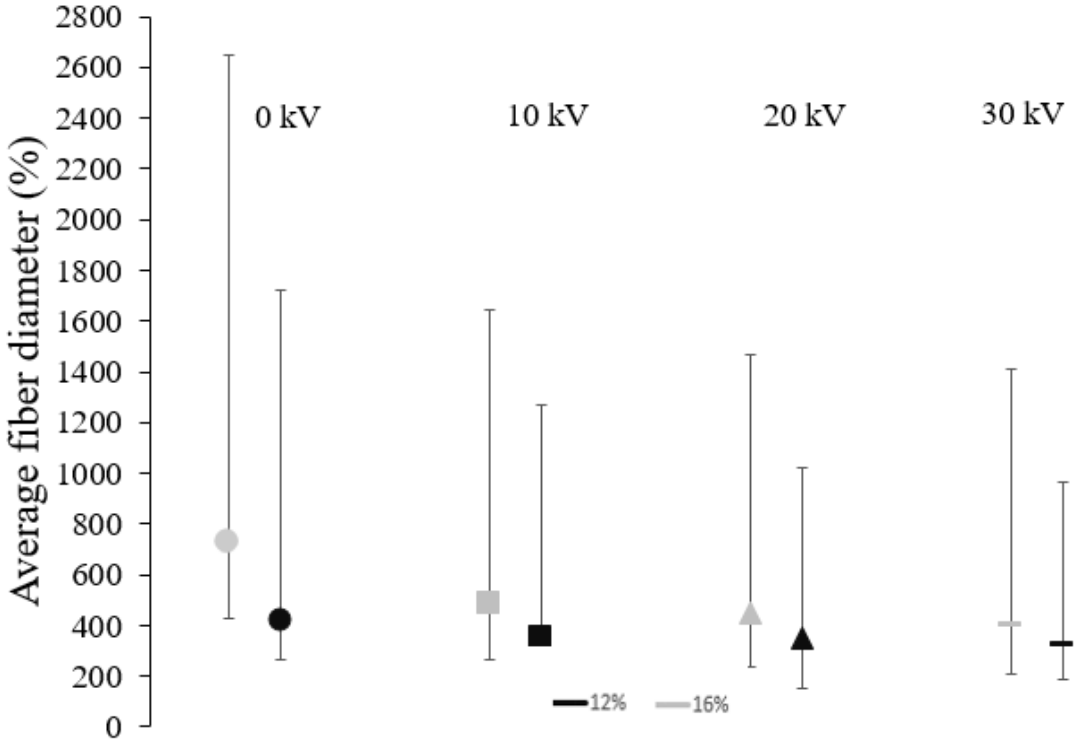

Figure 4.4: Average fiber diameter as a function of electric voltage at different solution concentrations (12 and 16wt.%).

Table 4.2: AFD and their corresponding statistical results at 12 and 16 wt.%.

Sample code	Maximum diameter (nm)	Average fiber diameter (nm)	Minimum diameter (nm)	Standard deviation (nm)
12-0_a	1297	424	162	233
12-10_a	919	347	153	152
12-20_a	673	349	195	120
12-30_a	637	328	141	105
16-0_b	1923	727	300	366
16-10_b	1163	482	214	184
16-20_b	1018	448	212	170
16-30_b	1006	408	202	143

a and b refer to the produced samples with 12 wt.% and 16 wt.% PVDF solutions.

4.1.3 Pore size distribution

Pore size distributions of 12 wt.% spun nanofibrous membranes produced at different electric voltage of 10, 20, and 30 kV are shown in Table 4.3. Results show that the mean flow pore size decreases with the increase of electrical voltage. Similar finding has been seen in one study that utilized ES as the production method [83]. This suggests that with high electric voltage the fibers are packed more closely and forming lower pore size, which is a very practical point of view in air filtration development.

Table 4.3: Pore size distribution at high electric voltage.

Electric voltage (kV)	Min pore size (µm)	Mean pore size (µm)	Max pore size (µm)
10	2.56	3.43	6.98
20	2.20	3.12	8.03
30	1.50	2.50	7.22

4.1.4 Filtration efficiency

Filtration efficiency and quality factor measurement results are summarized in Figure 4.5 and Figure 4.6. The filtration efficiency of the nonwoven on which is used as a substrate to collect the fibers is reported included as well.

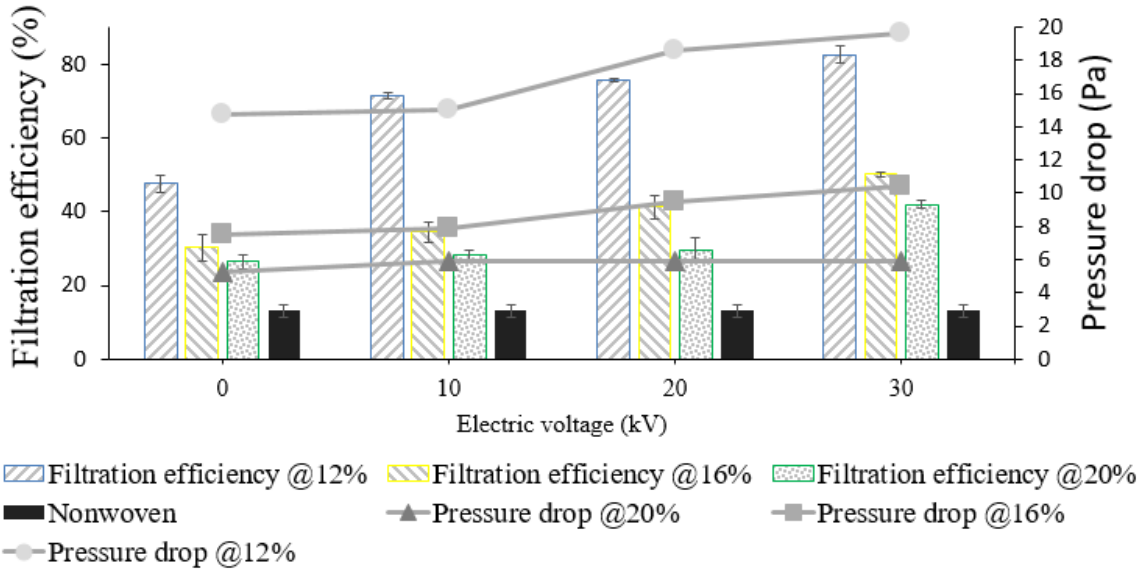

Figure 4.5: Filtration efficiency at a flow rate of 32 L/min under different electrical voltage (gsm ~ 0.8 $g.m^{-2}$).

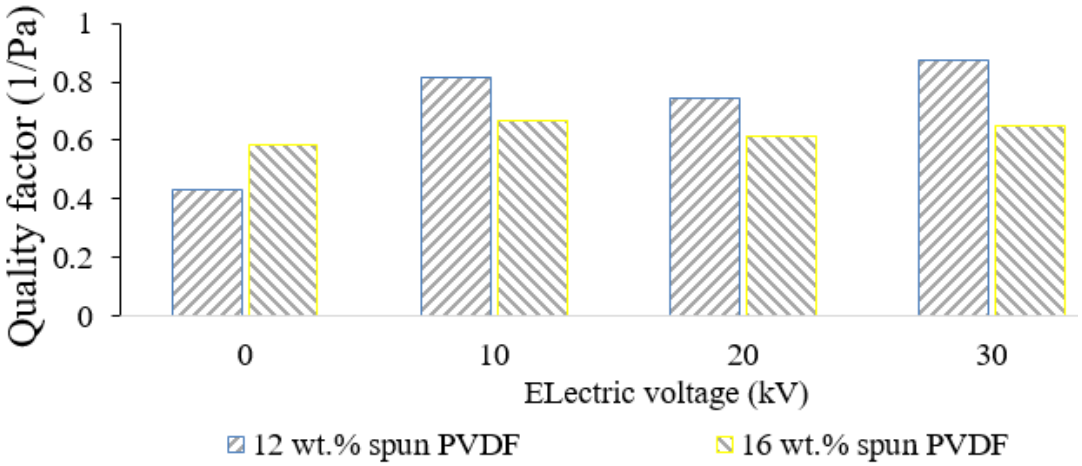

Figure 4.6: The quality factor of the 12% and 16% spun solutions at electric voltages 0 kV, 10 kV, 20 kV, and 30 kV.

The solution concentration plays a critical role in defining the filtration efficiencies of the spun nanofibrous membrane. This filtration efficiency-solution concentration relationship shows at the lower concentrations the capturing efficiency was enhanced at the expense of increase of pressure drop. The reason is that AFD deceases and the perhaps pore size decreases too [83,84]. Here independent of electric voltage, e.g. when the electric voltage was constant at 10 kV the AFDs of 12 wt.% and 16 wt.% were 479 ± 185 and 358 ± 222 nm and that correspond to capturing efficiencies of 71.4 ± 1% and 34.4 ± 2.8 %, respectively. The same pattern continues to be the same for the rest of the other measurements.

Nonetheless, It is clear that electric voltage has the same significant effect on the filtration efficiency of all nanofibrous membrane produced by the different solution concentrations. Results show that the higher the electrical voltage the higher the filtration efficiency, and the higher the pressure drop regardless of the polymer concentration of the base material. For instance at 12 wt.% concentration when the electric voltage outputs are 0, 10, 20, and 30 kV the filtration efficiency and pressure drop values are 47.5, 71.4, 75.7, and 82.5 % and 14.7, 15, 18.6, and 19.6 Pa, respectively. The same finding has been reported somewhere else using ES [85]. This phenomenon is explained by the decreased AFD and fiber distribution that allows increasing further the specific surface area and that higher electric voltage promotes lower pore size.

In order to understand the performance of all the produced filter media, their quality factors were calculated according to equation (4.1)

$$Q = \frac{\ln(\frac{1}{P})}{\Delta p} \tag{4.1}$$

where P is the percentage of penetration of the particles, and Δp is the pressure drop across the filter media. The 12 wt.% concentration spun solution at 30 kV has the highest performance of a quality factor of 0.87 mmH_2O^{-1} among all the filter media membranes. Interestingly, unlike 12% spun membrane, the best filter performance that spun from 16% solution was at electric voltage of 10 kV and has a quality factor of 0.67 mH_2O^{-1}. This may be explained by the stepper increase of pressure drop at 20 and 30 kV and the low capturing efficiency at 0 kV.

In order to see the effect of electrostatic charges, the nanofibrous membranes were treated with IPA to eliminate the charges and then the filtration efficiency tests were repeated for those treated samples as shown in Figure 4.7. The electret property of the produced filter membranes using ESBS is evident by the decrease of filtration efficiency after charge elimination. Electrostatic capturing efficiency is shown in Figure 4.8. Moreover, the 12 wt.% spun membranes have lower electret property when electric voltage increases. On the contrast, with 16 wt.% spun membranes the electret property increases with the increase of electric voltage.

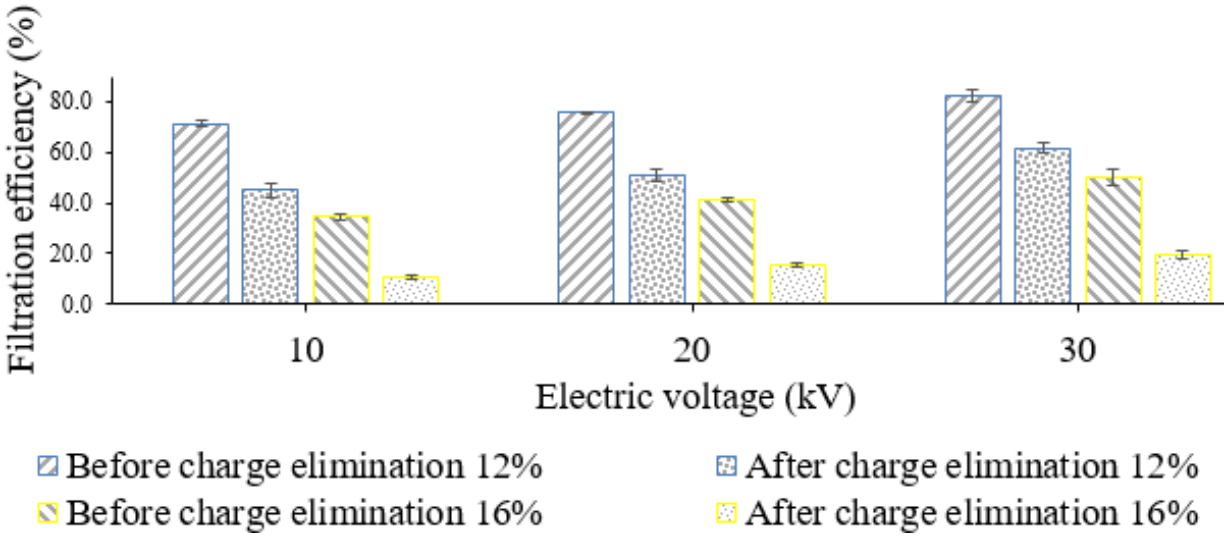

Figure 4.7: Filtration efficiency before and after charge elimination for 12 and 16 wt.% spun nanofibrous membranes.

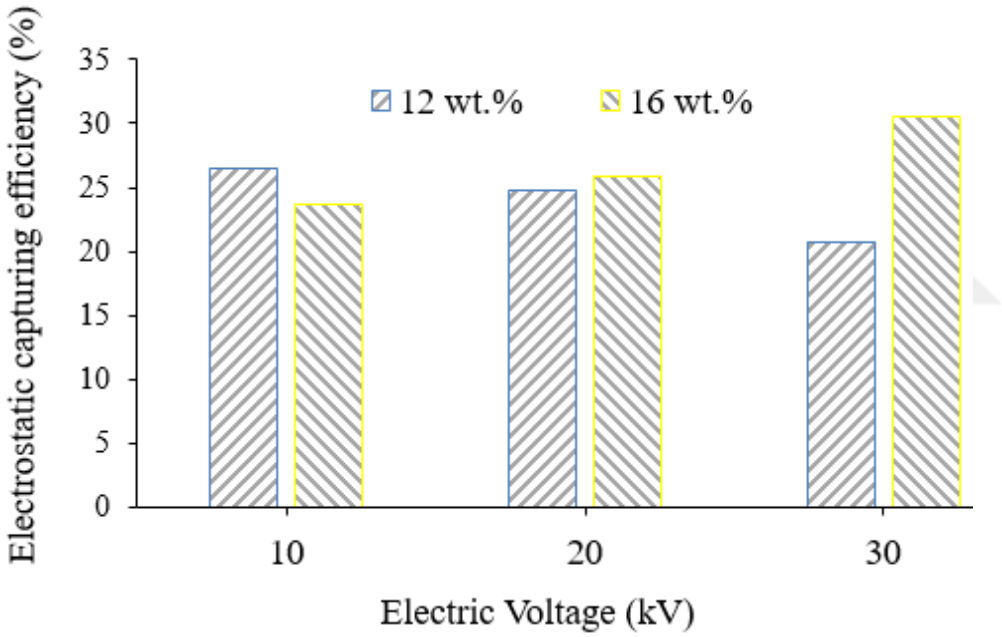

Figure 4.8: Electrostatic capturing efficiency of nanofibrous membranes produced from 12 and 16 wt.% solutions.

Filtration properties of a variety of methods of different as spun polymeric nanofibrous membranes are summarized in Table 4.4. These different nanofibrous membranes from literature are compared with the developed nanofibrous membrane in this work that was spun from 12 wt.% PVDF concentration at electric voltage of 30 kV. Generally, the developed nanofibrous membranes are promising compared with others produced via different methods.

Table 4.4: Comparision with as spun different polymeric based nanofibrous and membranes developed via a variety of methods.

Method	Base material	Basis weight ($g.m^{-2}$)	AFD (nm)	Flow rate (L/m)	Filtration efficiency (%)	Pressure drop (Pa)	Reference
Meltblowing	PP	24.8	520	32	82.5	57.9	[86]
ES	PVDF	20		10	93.8	983.9	[87]
ES	PAN	-	600-700	85	62.0	44.3	[39]
ES	PAN	~0.5	~270	32	~64.0	~9.0	[88]
ES	PVDF	-	622	-	~77.0	~17	[83]
SBS	PA 6	15.6	193	32	93.5	30.4	[82]
ESBS	PVDF	~0.8	328	2	82.5	19.6	This work

4.2 Development Of Nanofibrous Membrane As Separator In LIB

4.2.1 Rheological behavior of the solutions

Modacrylic and hydrophilic SiO_2 NPs were blended with co-PVDF solutions at a constant concentration of 13%. The solution properties, blending ratios and viscosity results are shown in Table 4.5. Results show that with the addition of modacrylic the viscosity increases, which this might be related to the high molecular weight of modacrylic. The same observation is noticed with the addition of NPs [67,73]. With as little as 0.1 wt.% of SiO_2 added to 50:50 co-PVDF/modacrylic the viscosity increases from 759 up to 981 mPa.s.

Table 4.5: Rheological behavior of co-PVDF and its blends.

Blend ratio (co-PVDF/Modacrylic)	SiO_2 (wt.%)	Solvent ratio (DMF/Acetone)	Viscosity (mPa.s)
100:0	0	70:30	382
75:25	0	70:30	521
50:50	0	70:30	759
25:75	0	70:30	1041
50:50	0.1	70:30	981
50:50	1	70:30	1044
50:50	10	70:30	1516

4.2.2 Surface morphology analysis

The effect of the addition of modacrylic on the morphology using SEM is shown in Figure 4.9 and their corresponding statistical results are shown in Table 4.6. Results show that the addition of modacrylic has enhanced the morphology extensively. This might suggest that modacrylic has better spinnability than co-PVDF does. This enhancement is evaluated based on less number of the defects (islands and beads) from SEM images. The defects become less frequent with a modacrylic content of 25%,

rarely observed with the modacrylic content of 50%, and completely gone when the modacrylic content reaches s75%.

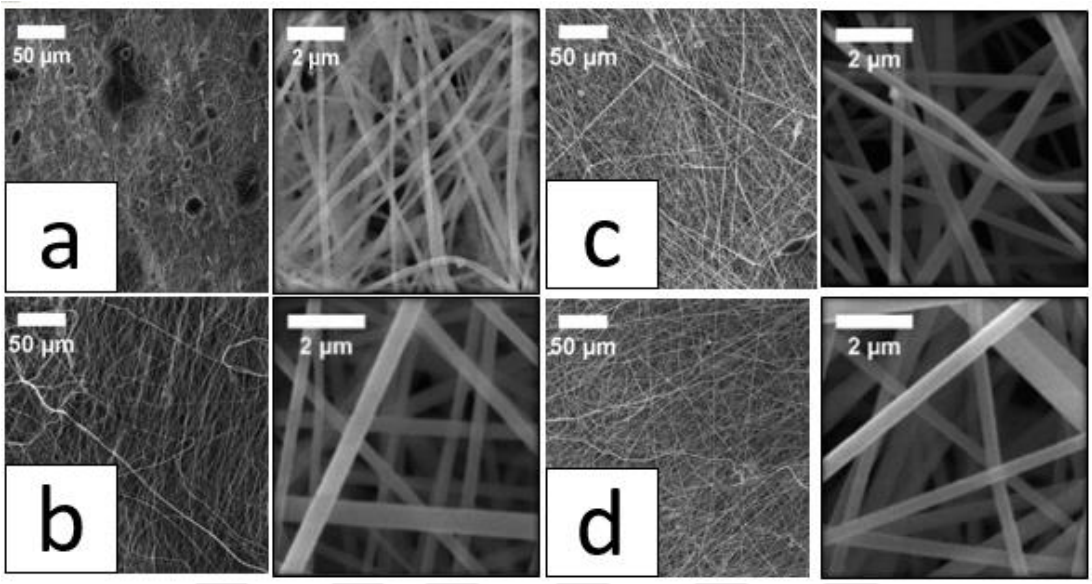

Figure 4.9: SEM images at 100 and 500 magnifications of nanofibrous membrane prepared from different co-PVDF/modacrylic blend ratio of: a) 100:0, b) 75:25, c) 50:50, and d) 25:75.

AFDs were calculated using ImageJ software. The AFDs as a function of viscosity are shown in Figure 4.10. Results show that with the increase of modacrylic content the AFD increases. A similar finding is reported; however, with the addition of PAN to PVDF [59].

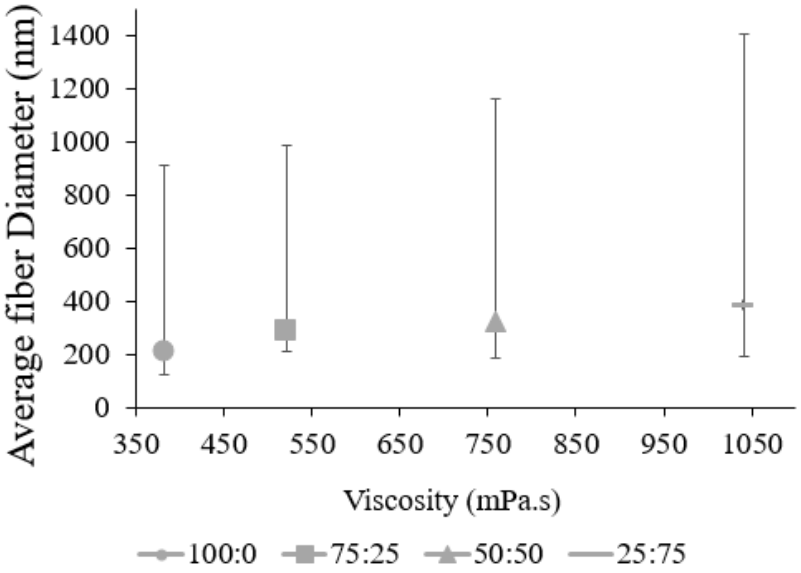

Figure 4.10: Average fiber diameter as a function of modacrylic content.

Table 4.6: AFD and their corresponding statistical results at different co-PVFD/modacrylic blend ratios.

Sample code	Maximum diameter (nm)	Average fiber diameter (nm)	Minimum diameter (nm)	Standard deviation (nm)
$100:0_a$	700	211	90	85
$25:75_a$	700	286	79	130
$50:50_a$	835	323	139	111
$25:75_a$	1015	388	194	114

a refers to the blend ratio of co-PVDF/modacrylic

Moreover, morphology results with the addition of SiO_2 NPs to 50:50 co-PVDF/modacrylic show that the morphology stays the same up to 1 wt.% of SiO_2 and then at 10 wt.% extremely big film-type structures can be observed. For that reason, this sample (with 10 wt.% SiO_2 NPs) has been excluded from any further separator related tests. This might be due to the high viscosity of the solution as Table 4.6 shows. SEM images of the addition of SiO_2 are shown in Figure 4.11.

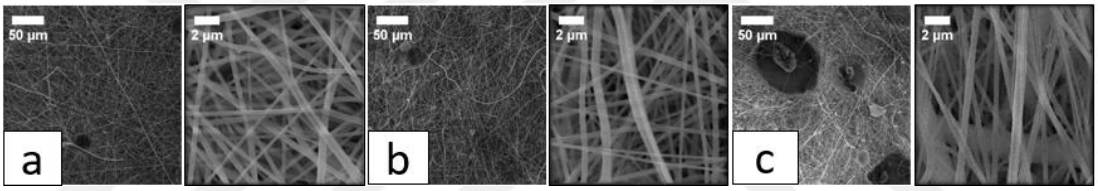

Figure 4.11: SEM images at 100 and 500 magnifications of nanofibrous membrane prepared with a blend ratio of 50:50 of co-PVDF/modacrylic containing: a) 0.1 wt.%, b) 1 wt.%, and c)10 wt.%

The relationship between AFD and viscosity before and after the addition of SiO_2 is depicted in Figure 4.12 and AFD their corresponding statistical results are shown in Table 4.7. The AFD increases slightly with the addition of SiO_2 NPs from 323 ± 111 (with 0 SiO_2 content) to 345 ± 108, 345 ± 140, and 384 ± 121 nm (with 0.1 wt.%, 1 wt.% and 10 wt.% content respectively). Similar results, however, with the addition of hydrophilic SiO_2 NPs to plain co-PVDF solution were reported somewhere else [67].

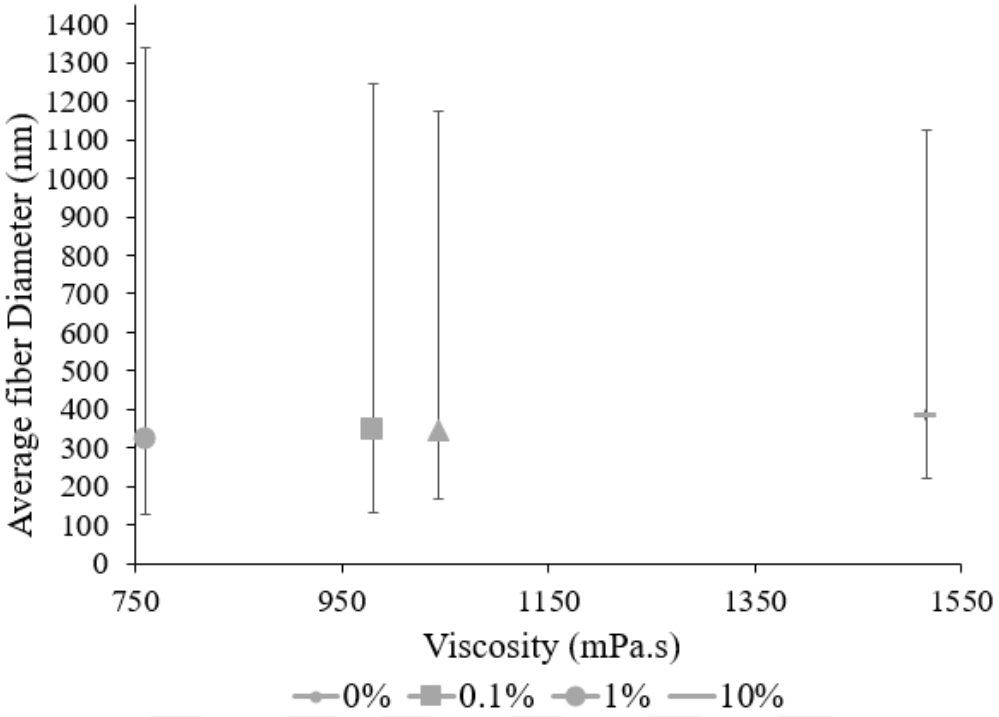

Figure 4.12: Average fiber diameter as a function of SiO2 content.

Table 4.7: AFD and their corresponding statistical results at different co-PVFD/modacrylic blend ratios.

Sample code	Maximum diameter (nm)	Average fiber diameter (nm)	Minimum diameter (nm)	Standard deviation (nm)
$50:50:0.1_a$	900	384	213	121
$50:50:1_a$	829	345	177	140
$50:50:10_a$	739	345	162	108

a refers to the blend ratio of co-PVDF/modacrylic/SiO_2.

4.2.3 Porosity

This test was conducted in order to define the porosity of the produced samples and the commercial PP separator. Table 4.8 shows the porosity results of all the produced samples. Results show the superiority of the nanofibrous membranes over the commercial one in terms of porosity, which is normal for non-nanofibrous membrane.

Table 4.8: Porosity results of the produced nanofibrous membrane and an available commercial separator.

Base material	Average porosity (%)	Standard deviation (%)
$100:0_a$	79	3
$75:25_a$	86	1
$50:50_a$	89	1
$25:75_a$	91	1
$50:50:0.1_b$	91	1
$50:50:1_b$	92	1
PP 2500	57	0

a refers to the blend ratio of co-PVDF/modacrylic and b refers to blend ratio of co-PVDF/modacrylic/SiO_2

Now, the result shows that higher content of modacrylic leads to higher porosity. This can be explained by the increasing ADFs with the increase of the modacrylic content. In order to clarify this relationship, a graph of porosity as a function of AFD is given in Figure 4.13.

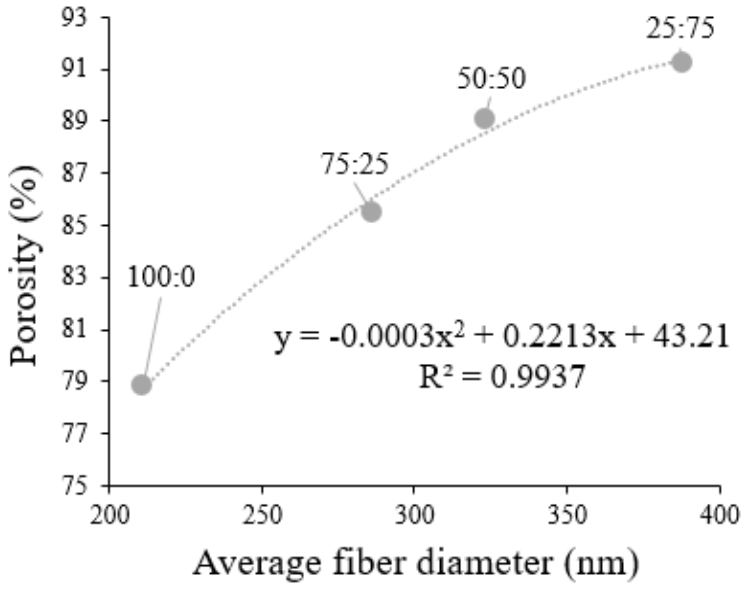

Figure 4.13: Porosity as a function of AFD with the addition of Modacrylic.

The addition of hydrophilic SiO_2 NPs has increased the porosity. This increase was from 89 ± 1% (with no SiO_2 content) to 91 ± 1 and 92 ± 1% when SiO_2 contents were 0.1% and 1%, respectively. Since the AFD with the addition of SiO_2 has not increased much (from 323 nm without SiO_2 content to 345 nm when SiO_2 content was 0.1 and 1 wt.%), it can be inferred that at this case the increase of the porosity was mainly due to SiO_2 content. The same finding has been reported in one study before [67,73]. All

and all, these high porosity results might suggest that the produced sample have a uniform fibril structure.

4.2.4 Wettability

The chosen electrolyte was $LiPF_6$ solution is widely used as commercially mainly due to its capability of providing high ionic conductivity and being electrochemically stable.

4.2.4.1 Electrolyte uptake

This test was carried to define the affinity of the produced separators and the available commercial separator to the used electrolyte. Table 4.9 shows the electrolyte uptake results of the separators and the developed separator in this thesis. The commercial separator has an uptake of 59 ± 4%, which is trivial compared with the electrolyte of the developed separators. The high values of these nanofibrous membranes are the result of their high porosity [50,51,89,90].

Table 4.9: Average electrolyte uptake.

Base material (co-PVDF/Modacrylic/SiO_2)	Average electrolyte uptake (%)	Standard deviation (%)
$100:0_a$	343	30
$75:25_a$	362	15
$50:50_a$	417	23
$25:75_a$	517	30
$50:50:0.1_b$	539	50
$50:50:1_b$	606	29
PP 2500	59	4

a refers to the blend ratio of co-PVDF/modacrylic and b refers to blend ratio of co-PVDF/modacrylic/SiO_2

To illustrate why the co-PVDF/modacrylic membranes have such high electrolyte uptake compared with the commercial separator of which has a porosity of only 57%, the electrolyte uptake as a function of the porosity is given in Figure 4.14. It is safe to infer that higher porosity helps to hold in more of the electrolyte within its empty voids. This result indicts the significance of nanofibrous membrane due to its outstanding ability to provide high porosity in which holds in more electrolyte.

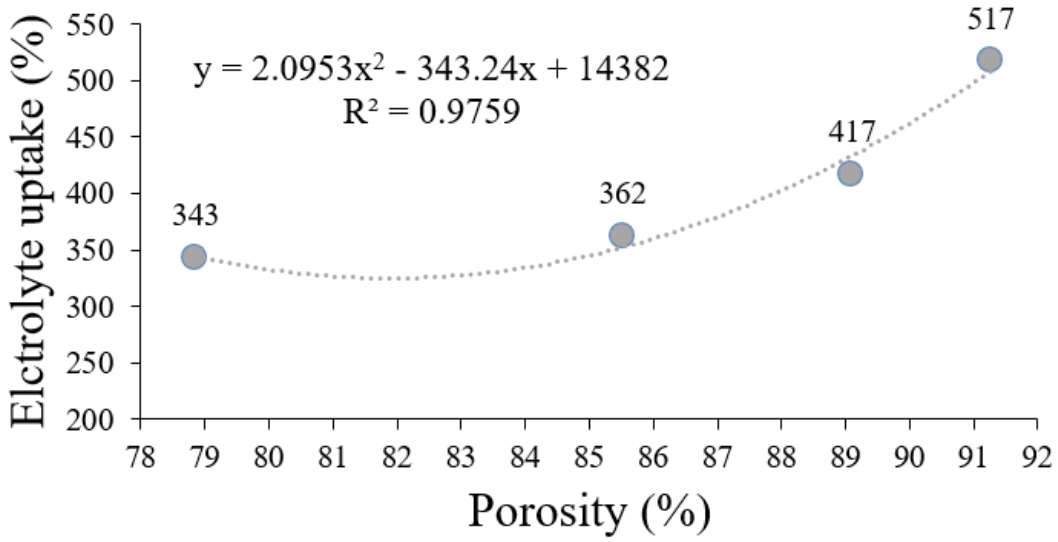

Figure 4.14: Electrolyte uptake as a function of porosity.

In order to understand the effect of SiO_2 content on electrolyte uptake, electrolyte uptake and porosity as functions of SiO_2 content is given in Figure 4.15. Results show the strong correlation between electrolyte uptake and porosity. The SiO_2 content plays a significant role in determining porosity and, therefore, electrolyte uptake. The electrolyte uptake increases from 417 to 539 and 606% with the slightest increase of SiO_2 content from 0, 0.1 and 1 wt.%, respectively. Porosity also increases from 88, 91, and 92% with the increase of SiO_2 content from 0, 0.1, and 1 wt.%, respectively. Results also suggest that with SiO_2 content of 0.1 wt.% it is enough to significantly enhance both electrolyte uptake and porosity.

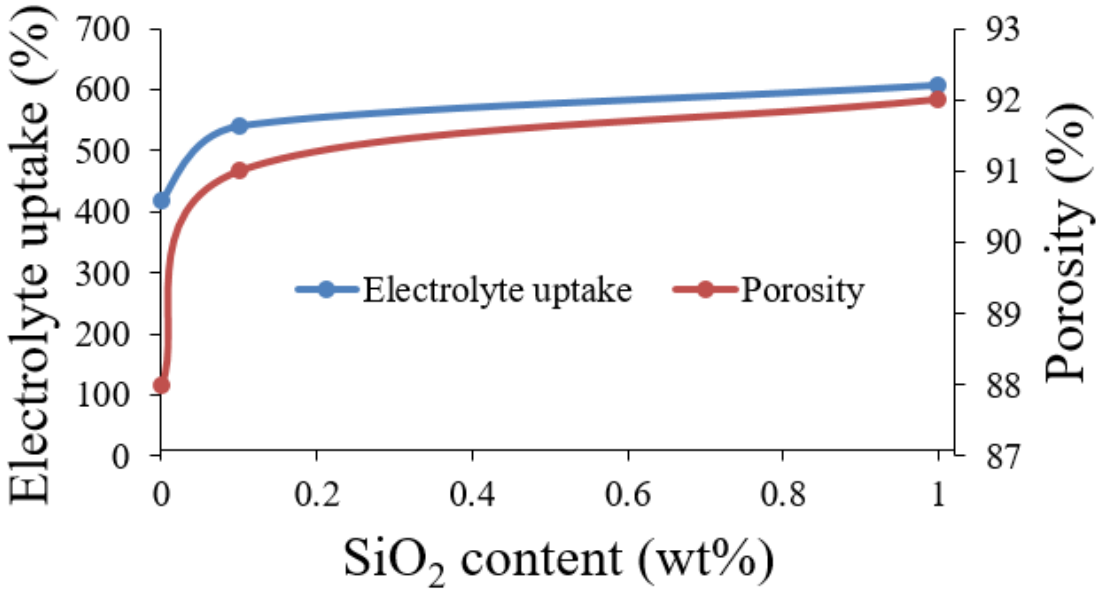

Figure 4.15: Electrolyte and porosity as a function of SiO_2 content.

4.2.4.2 Contact angle

This test serves as a complementary tool to further emphasize the difference in wettability between the membranes that are used in LIBs as separators. A droplet of 5 µL of LiPF6 was dropped on a coin size separator to measure its average contact angle (ACA). Since the developed separators show very high affinity to the electrolyte, 5 seconds was sufficient as the time it takes to measure the contact angle (to fully be absorbed). Table 4.10 shows the ACA and other related statistical results. Results show Celgrad PP 2500 has ACA of around 77º while the largest ACA of the developed separators was almost 14º when co-PVDF/modacrylic content was 25:75. Moreover, the ACA decreases after the addition of hydrophilic SiO2 NPs from 13º (co-PVDF/modacrylic of 50:50) to 9.6 and 8.8º at which the content of SiO2 (co-PVDF/modacrylic/SiO2) was 0.1 and 1 wt.%, respectively. To illustrate the above, the contact angle measurement and digital images of 5 µL droplet on the PP separator and co-PVDF/modacrylic/SiO2 of 50:50:1 wt.% are shown in Figure 4.16.

Table 4.10: Average contact angle and statistical measurements.

Measurement	Celgrad PP 2500	100:0	75:25	50:50	25:27	50:50:0.1 wt.%	50:50:1 wt.%
Average contact angle	77.1	11.6	12.9	13.0	13.8	9.6	8.8
Standard deviation	1.7	3.6	3.6	3.3	3.3	4	3.8
Minimum	74.1	7.8	8.6	8.7	8.7	4.6	5.2
Maximum	80.6	23.9	28.1	29.0	29.0	23.0	27
Mean time	5	2.3	2.5	2.2	2.2	1.5	2.3

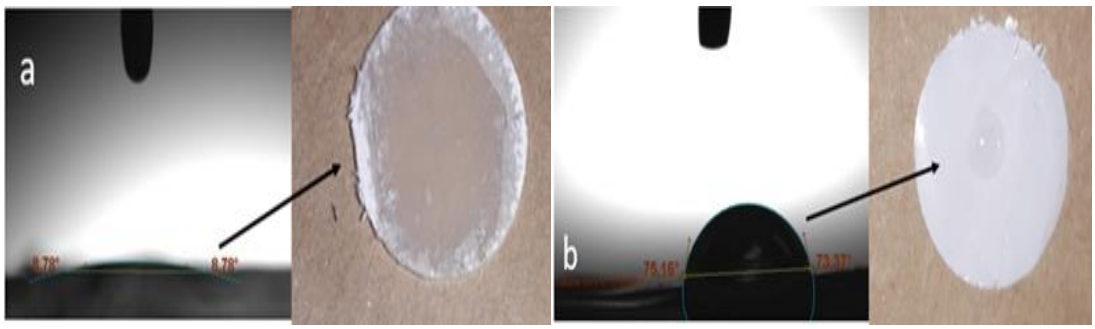

Figure 4.16: Measurements of contact angle of co-PVDF/modacrylic/SiO_2 of 50:50:1 wt.%nanofibrous membrane and b) the Celgrad PP 2500 commercial separator.

4.2.5 Thermal properties

4.2.5.1 Dimensional stability

The dimensional stability of the developed nanofibrous membranes and the commercial PP separator was evaluated by determining the thermal shrinkage rate at 140 °C for 1 hour using equation 2. Results are shown in Table 4.11. The addition of modacrylic enhances dimensional stability because it has a higher melting point (~250 °C) than co-PVDF (~150 °C). In one study, similar results were obtained with the addition of PAN with PVDF [55]. On the other hand, since these hydrophilic SiO_2 NPs have a thermal resistance of 850 °C, they increase the entire thermal resistance of the nanofibrous membrane with only 0.1 wt.% of NPs [66]. When, however, SiO_2 becomes 1 wt.% the overall thermal shrinkage decreases for which this might be related to the decreased crystallinity of the nanofibrous membrane [66]. By contrast, the commercial PP separators are not stable and curl up as Figure 4.17 shows, which they might cause serious safety issues if the battery undergoes higher temperatures.

Table 4.11: Thermal shrinkage rate with for the developed nanofibrous membranes and PP commercial separator.

Material	Transverse direction (%)	Machine direction (%)
$100:0_a$	~63	~71
$75:25_a$	9 ± 1	9 ± 3
$50:50_a$	3 ± 1	3 ± 1
$25:75_a$	1 ± 1	1 ± 2
$50:50:0.1_b$	1 ± 1	1 ± 1
$50:50:1_b$	3 ± 1	3 ± 2
PP 2500	Unstable and curl up	Unstable and curl up

a refers to the blend ratio of co-PVDF/modacrylic and b refers to blend ratio of co-PVDF/modacrylic/SiO_2.

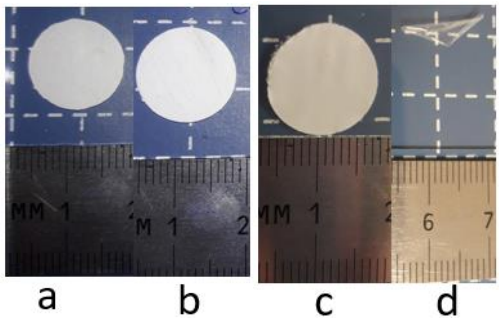

Figure 4.17: Thermal shrinkage rate at 140 °C for 1 h: a and c before treatment and b and d after treatment for Celgrad PP 2500 and 50:50/0.1.wt% SiO_2 of co-PVDF/modacrylic, respectively.

4.2.5.2 Combustion behavior

A combustion test is a complementary test to further evaluate the thermal stability of a separator in LIB [91]. Figure 4.18 shows the combustion test of different polymeric based nanofibrous and porous membranes. Of these polymeric based nanofibrous materials, a solution blown PAN-based nanofibrous membrane was used. The test was carried out by subjecting the membranes to a close source of fire for a few seconds. Results show PAN-based nanofibrous membrane caught fire easily and burst into flames very rapidly, while PP-based membrane shrunk immediately. These observations are related to the poor flame retardant property of both PAN and PP and the low melting point of PP [92]. Though PVDF-based nanofibrous membrane does not catch fire, it severely shrank. This is mainly due to its flame retardant property and low melting point [74]. According to Figure 4.19 (e), PVDF/modacrylic-based nanofibrous membrane exhibits the best flame retardant property compared with the other membranes, which is due to its flame retarding property [93].

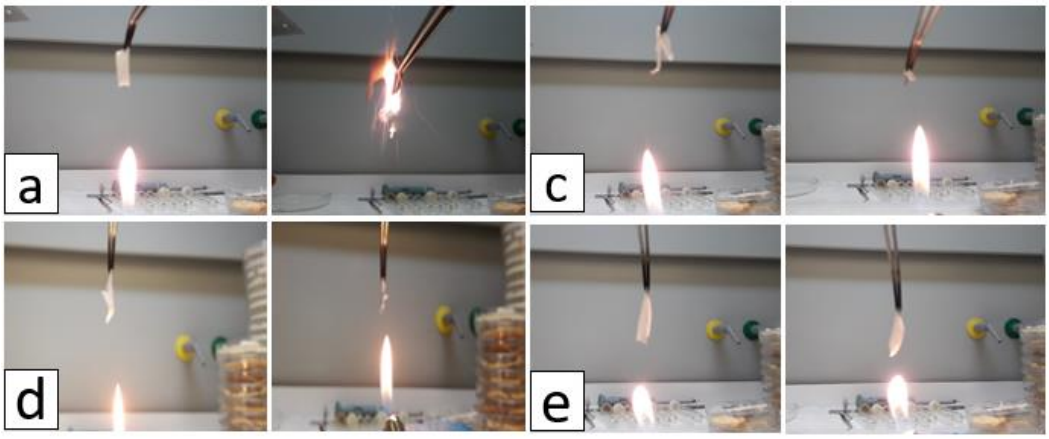

Figure 4.18: Combustion test of nanofibrous membrane based a) PAN, b) PP, c) PVDF, and e) PVDF/modacrylic.

4.2.6 Mechanical property

Acceptable mechanical properties manifest with the tensile strength and elongation, which are two of the basic requirements of a separator in LIB because the separator needs to bear the right amount of tension and elongation during winding with electrodes. Worth mentioning that tensile strength is more significant in the machine direction than the transverse direction [61]. Here the mechanical test was conducted only on the machine direction. Figure 4.19 shows the mechanical properties of the

developed samples. The addition of modacrylic does not seem to change the tensile strength significantly. In fact, the addition of modacrylic seems to have a random effect on the mechanical strength of the material. PVDF/modacrylic-based nanofibrous membranes of ratios of 75:50 and 50:50 have the highest and the lowest tensile strength of 2.68 and 2.31 MPa, respectively. Similar findings were reported elsewhere after the addition of PAN to PVDF-based nanofibrous membranes [54]. Now, after the addition of SiO_2 NPs, the tensile strength increases but elongation slightly decreases. This enhancement of tensile strength was more pronounced after the addition of 1 wt.% of SiO_2 at 2.8 MPa. In one study, the addition of SiO_2 NPs to a PVDF/PAN-based nanofibrous membrane showed similar behavior to the developed nanofibrous with SiO_2 NPs in this work [94]. These NPs play a role of reinforcing the polymer matrix [53]. Generally, the addition of modacrylic enhances the flexibility of the nanofibrous membrane and the addition of SiO_2 nanoparticles reinforce the polymer matrix, which results in higher tensile strength at the expense of flexibility.

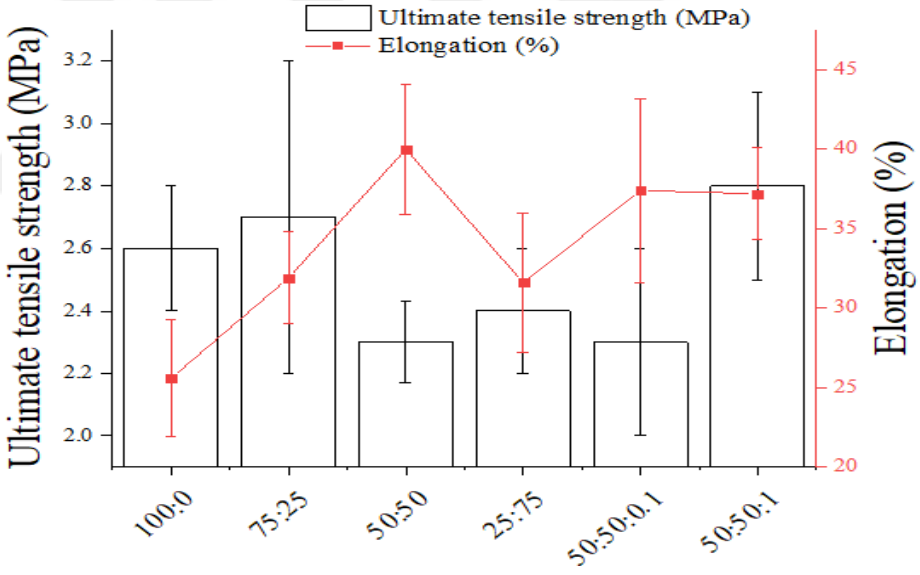

Figure 4.19: Mechanical properties of different nanofibrous membranes.

Moreover, the thicknesses of the membranes are reported in Table 4.12.

Table 4.12: Thicnkess measurment of differnet developed membranes.

Material	Thickness (µm)
$100:0_a$	16 ± 1
$75:25_a$	41 ± 3
$50:50_a$	41 ± 1
$25:75_a$	46 ± 2
$50:50:0.1_b$	42 ± 2
$50:50:1_b$	55 ± 4

4.2.7 Ionic conductivity

The ionic conductivity was deduced from the measurement that was done by electrochemical impedance spectroscopy. Fig. 4.20 shows Nyquist plots drawn from EIS measurements.

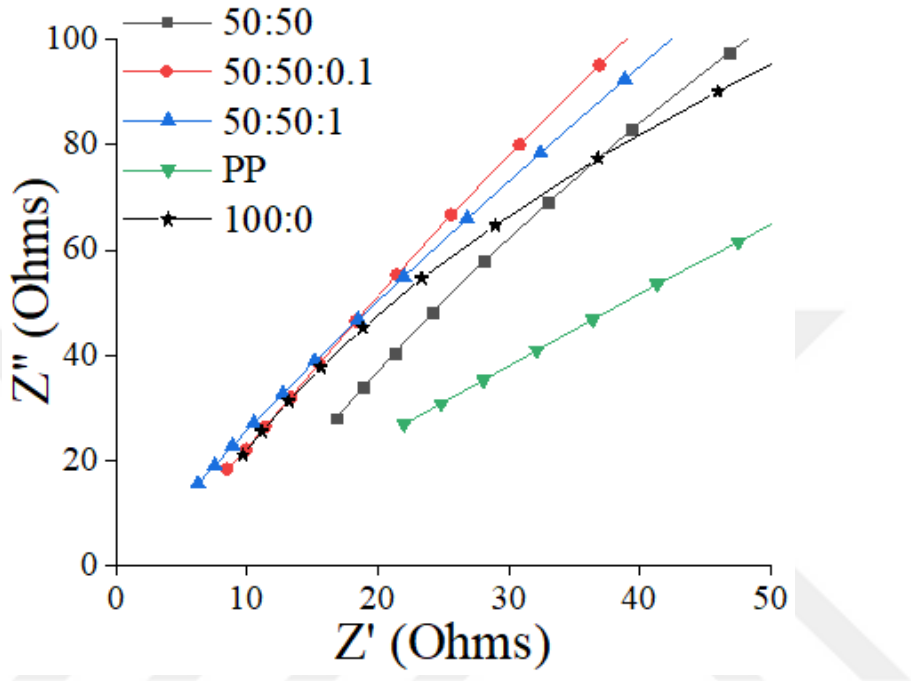

Figure 4.20: Electro impedance results of soaked separators with electrolyte solutions.

Results reveal co-PVDF/modacrylic possesses higher ionic conductivity than PP membrane, 0.51 and 0.18 $mS.cm^{-1}$, respectively as shown in Table 4.13. This might be attributed to the high porosity, electrolyte uptake, and the high affinity to the electrolyte solution. As has been established in the literature, the addition of hydrophilic SiO_2 increases the ionic conductivity to 1.34 and 3.67 $mS.cm^{-1}$ at 0.1 and 1 wt.% of SiO_2, respectively.

Table 4.13: Ionic conductivity results.

Material	Ionic conductivity ($mS.cm^{-1}$)
100:0	0.77
50:50	0.55
50:50:0.1	1.34
50:50:1	3.67
PP 2500	0.18

5. CONCLUSION AND FUTURE WORK

5.1 Conclusion

Electrically-assisted solution blow spinning technique has been employed to fabricate multi-purpose nanofibrous membranes for the aerosol filter (environmental) and as a separator in LIB (energy) applications.

The environmental application was realized in aerosol air filtration. At different conditions (PVDF concentration of 12 and 16 wt.% and electrical voltage of 0, 10, 20, and 30 kV) PVDF-based nanofibrous membranes as air filtration membranes were developed and characterized for air filtration purpose. The developed nanofibrous membranes of both PVDF concentrations are suitable to be used as filter membranes. Filtration efficiencies are prominent at 12 wt.% concentration and high electric voltage outputs due to small nanofibers (347, 349, and 328 nm at 10, 20, and 30 kV, respectively) small pore size (3.4, 3.1, and 2.5 μm at 10, 20, and 30, respectively). Decreasing solution concentration yields lower fiber diameters, while increasing electric voltage output fiber diameters and pore size decrease and therefore, they enhance capturing efficiency (71.4%, 75.7%, and 82.5% at 10 kV, 20 kV, and 30 kV, respectively) and filter performance as well. It is concluded that ESBS is capable of introducing electret property upon the produced samples at high electric voltages. The highest electrostatic capturing efficiency of 26.5 and 30.5 % of 12 and 16 wt.% spun solutions, respectively, were reported at electric voltage of 10 and 30 kV, respectively. The system has shown its capability to produce nanofibrous membranes with a huge control over their specifications at a high production rate. The aforementioned findings are generalized and listed below:

- Lower concentration yields smaller nanofibers.
- Higher electric voltage yields smaller nanofibers and pore sizes.
- Smaller nanofibers and pore size enhance mechanical capturing mechanism.

- Electric voltage provides electrostatic charges, and thus, enhances electrostatic capturing mechanism.

On the other hand, energy application was realized with the development of nanofibrous membranes in LIBs. Combinations of co-PVDF/Modacrylic/SiO_2 based nanofibrous membranes were developed and characterized as separators in LIB. The addition of Modacrylic enhanced porosity (from 79% with a blend ratio of 100:0 to 86%, 89%, and 91% with blend ratios of 75:25, 50:50 and 25:75) and as a result, improved electrolyte uptake (from 343% to 517%). Porosity and electrolyte uptake was further enhanced with the addition of a tiny amount of SiO_2 (porosity increased from 88% to 92% and electrolyte uptake increased from 417% to 606%). Wettability with all combination of co-PVDF/Modacrylic/SiO_2 is superior over available commercial PP separators. Moreover, Modacrylic, benefiting from its high melting point, has increased the dimensional stability of the co-PVDF/Modacrylic blend (less than 5% with a blend ratio of 50:50 and above). This enhancement of dimensional stability was improved with the addition of only 0.1 wt.% of SiO_2. In a nutshell, co-PVDF/Modacrylic/SiO_2 developed with ESBS facilitated high functional separators in LIBs at a high production rate. The aforementioned findings of the second chapter are generalized and listed below:

- Larger nanofiber diameters promote higher porosity.
- Nanofibrous membranes possess high porosity.
- Nanofibrous membranes retain high electrolyte uptake.
- Modacrylic content enhances spinnability, dimensional and thermal stabilities, and mechanical property.
- Nanofibrous membranes enhance ionic conductivity.
- Addition of hydrophilic SiO_2 NPs enhances porosity, ionic conductivity, and mechanical property.

5.2 Future Work

Since the developed nanofibrous membranes for aerosol filtration have shown electret properties, then it is essential to study their surface potential stability and longevity. These two factors are the most important and challengeable when it comes to developing electret filter membranes. Nonetheless, when polymeric separators consist of inorganic material, such as SiO_2, in the metal-lithium battery, they usually suffer from dendrites that limit their performance. For that, developing a sandwich structure made of co-PVDF/modacrylic as skin layers and co-PVDF/modacrylic/SiO_2 as a middle layer might worth one's time to research and investigate.

REFERENCES

[1] **Mikulášek, P. and Cuhorka, J.** (2017). 12 - Application of nanofibrous membranes and their suitability for membrane bioreactor processes in wastewater treatment. in: P.J. Brown, C.L. Cox (Eds.), Fibrous Filter Media, Woodhead Publishing, pp. 275–290.

[2] **Supaphol, P., Mit-Uppatham, C., and Nithitanakul, M.** (2005). Ultrafine electrospun polyamide-6 fibers: Effect of emitting electrode polarity on morphology and average fiber diameter. *Journal of Polymer Science Part B: Polymer Physics*, ***43***, 3699–3712.

[3] **Shahabadi, S.M.S., Kheradmand, A., Montazeri, V., and Ziaee, H.** (2015). Effects of process and ambient parameters on diameter and morphology of electrospun polyacrylonitrile nanofibers. *Polym. Sci. Ser. A*, ***57***, 155–167.

[4] **Yee, W.A., Kotaki, M., Liu, Y., and Lu, X.** (2007). Morphology, polymorphism behavior and molecular orientation of electrospun poly(vinylidene fluoride) fibers. *Polymer*, ***48***, 512–521.

[5] **Kim, I.-D., Rothschild, A., Lee, B.H., Kim, D.Y., Jo, S.M., and Tuller, H.L.** (2006). Ultrasensitive Chemiresistors Based on Electrospun TiO2 Nanofibers. *Nano Lett.*, ***6***, 2009–2013.

[6] **Choi, S.-S., Lee, S.G., Im, S.S., Kim, S.H., and Joo, Y.L.** (2003). Silica nanofibers from electrospinning/sol-gel process. *Journal of Materials Science Letters*, ***22***, 891–893.

[7] **Kim, J.-W., Cho, W.-J., and Ha, C.-S.** (2002). Morphology, crystalline structure, and properties of poly(vinylidene fluoride)/silica hybrid composites. *Journal of Polymer Science Part B: Polymer Physics*, ***40***, 19–30.

[8] **Radacsi, N., Campos, F.D., Chisholm, C.R.I., and Giapis, K.P.** (2018). Spontaneous formation of nanoparticles on electrospun nanofibres. *Nature Communications*, ***9***, 4740.

[9] **Agarwal, S., Jiang, S., and Greiner, A.** (2019). Chapter 4 - Nanofibrous Structures. in: B. Ding, X. Wang, J. Yu (Eds.), Electrospinning: Nanofabrication and Applications, William Andrew Publishing, pp. 93–122.

[10] **Kluge, D., Singer, J.C., Neubauer, J.W., Abraham, F., Schmidt, H.-W., and Fery, A.** (2012). Influence of the molecular structure and morphology of self-assembled 1,3,5-benzenetrisamide nanofibers on their mechanical properties. *Small*, ***8***, 2563–2570.

[11] **Bernet, A., Behr, M., and Schmidt, H.-W.** (2011). Supramolecular nanotube-based fiber mats by self-assembly of a tailored amphiphilic low molecular weight hydrogelator. *Soft Matter*, ***7***, 1058–1065.

[12] **Tokarev, A., Asheghali, D., Griffiths, I.M., Trotsenko, O., Gruzd, A., Lin, X., et al.** (2015). Touch- and Brush-Spinning of Nanofibers. *Advanced Materials*, ***27***, 6526–6532.

[13] **Doshi, J. and Reneker, D.H.** (1995). Electrospinning process and applications of electrospun fibers. *Journal of Electrostatics*, ***35***, 151–160.

[14] **Al-Attabi, R., Dumée, L.F., Schütz, J.A., and Morsi, Y.** (2018). Pore engineering towards highly efficient electrospun nanofibrous membranes for aerosol particle removal. *Sci. Total Environ.*, ***625***, 706–715.

[15] **Park, J.Y., Lee, I.H., and Bea, G.N.** (2008). Optimization of the electrospinning conditions for preparation of nanofibers from polyvinylacetate (PVAc) in ethanol solvent. *Journal of Industrial and Engineering Chemistry*, ***14***, 707–713.

[16] **Tsai, P.P., Schreuder-Gibson, H., and Gibson, P.** (2002). Different electrostatic methods for making electret filters. *Journal of Electrostatics*, ***54***, 333–341.

[17] **Varesano, A., Carletto, R.A., and Mazzuchetti, G.** (2009). Experimental investigations on the multi-jet electrospinning process. *Journal of Materials Processing Technology*, ***209***, 5178–5185.

[18] **Reneker, D.H. and Chun, I.** (1996). Nanometre diameter fibres of polymer, produced by electrospinning. *Nanotechnology*, ***7***, 216–223.

[19] **Lu, Y., Li, Y., Zhang, S., Xu, G., Fu, K., Lee, H., et al.** (2013). Parameter study and characterization for polyacrylonitrile nanofibers fabricated via centrifugal spinning process. *European Polymer Journal*, ***49***, 3834–3845.

[20] **Sinha-Ray, S., Sinha-Ray, S., Yarin, A.L., and Pourdeyhimi, B.** (2015). Theoretical and experimental investigation of physical mechanisms responsible for polymer nanofiber formation in solution blowing. *Polymer*, ***56***, 452–463.

[21] **Sinha-Ray, S., Yarin, A.L., and Pourdeyhimi, B.** (2010). Meltblowing: I-basic physical mechanisms and threadline model. *Journal of Applied Physics*, ***108***, 034912.

[22] **Yarin, A.L., Sinha-Ray, S., and Pourdeyhimi, B.** (2010). Meltblowing: II-linear and nonlinear waves on viscoelastic polymer jets. *Journal of Applied Physics*, ***108***, 034913.

[23] **Polat, Y., Pampal, E.S., Stojanovska, E., Simsek, R., Hassanin, A., Kilic, A., et al.** (2016). Solution blowing of thermoplastic polyurethane nanofibers: A facile method to produce flexible porous materials. *Journal of Applied Polymer Science*, ***133***,.

[24] **Zhang, L., Kopperstad, P., West, M., Hedin, N., and Fong, H.** (2009). Generation of polymer ultrafine fibers through solution (air-) blowing. *Journal of Applied Polymer Science*, ***114***, 3479–3486.

[25] **Kakoria, A. and Sinha-Ray, S.** (2018). A Review on Biopolymer-Based Fibers via Electrospinning and Solution Blowing and Their Applications. *Fibers*, ***6***, 45.

[26] **Lin, Y., Yao, Y., Yang, X., Shen, L., Li, R., and Wu, D.** (2009). Effect of gas flow rate on crystal structures of electrospun and gas-jet/electrospun poly(vinylidene fluoride) fibers. *Chinese J. Polym. Sci.*, ***27***, 511–516.

[27] **Bryner, M.A., Armantrout, J.E., Armstrong, J.E., and Johnson, B.S.** (2006). Improved electroblowing web formation process, WO2006071976A2, 2006.

[28] **He, M., Ichinose, T., Kobayashi, M., Arashidani, K., Yoshida, S., Nishikawa, M., et al.** (2016). Differences in allergic inflammatory responses between urban PM2.5 and fine particle derived from desert-dust in murine lungs. *Toxicol. Appl. Pharmacol.*, ***297***, 41–55.

[29] **Anderson, J.O., Thundiyil, J.G., and Stolbach, A.** (2012). Clearing the air: a review of the effects of particulate matter air pollution on human health. *J Med Toxicol*, ***8***, 166–175.

[30] **Sun, Q. and Leung, W.W.-F.** (2019). Charged PVDF multi-layer filters with enhanced filtration performance for filtering nano-aerosols. *Separation and Purification Technology*, ***212***, 854–876.

[31] (n.d.). Glass Fibre - an overview | ScienceDirect Topics.
[32] **Yang, C.** (2012). Aerosol Filtration Application Using Fibrous Media—An Industrial Perspective. *Chinese Journal of Chemical Engineering*, ***20***, 1–9.
[33] **Hutten, I.M.** (2007). CHAPTER 2 - Filtration Mechanisms and Theory. in: I.M. Hutten (Ed.), Handbook of Nonwoven Filter Media, Butterworth-Heinemann, Oxfordpp. 29–70.
[34] **Sundarrajan, S., Tan, K.L., Lim, S.H., and Ramakrishna, S.** (2014). Electrospun Nanofibers for Air Filtration Applications. *Procedia Engineering*, ***75***, 159–163.
[35] **Kosmider, K. and Scott, J.** (2002). Polymeric nanofibres exhibit an enhanced air filtration performance. *Filtration & Separation*, ***39***, 20–22.
[36] **Podgórski, A., Bałazy, A., and Gradoń, L.** (2006). Application of nanofibers to improve the filtration efficiency of the most penetrating aerosol particles in fibrous filters. *Chemical Engineering Science*, ***61***, 6804–6815.
[37] **Kilic, A., Russell, S., Shim, E., and Pourdeyhimi, B.** (2017). 4 - The charging and stability of electret filters. in: P.J. Brown, C.L. Cox (Eds.), Fibrous Filter Media, Woodhead Publishing, pp. 95–121.
[38] **Kilic, A., Shim, E., Yeom, B.Y., and Pourdeyhimi, B.** (2013). Improving electret properties of PP filaments with barium titanate. *Journal of Electrostatics*, ***71***, 41–47.
[39] **Wang, N., Si, Y., Wang, N., Sun, G., El-Newehy, M., Al-Deyab, S.S., et al.** (2014). Multilevel structured polyacrylonitrile/silica nanofibrous membranes for high-performance air filtration. *Separation and Purification Technology*, ***126***, 44–51.
[40] **Scrosati, B.** (1992). Lithium Rocking Chair Batteries: An Old Concept? *J. Electrochem. Soc.*, ***139***, 2776–2781.
[41] **Costa, C.M., Silva, M.M., and Lanceros-Méndez, S.** (2013). Battery separators based on vinylidene fluoride (VDF) polymers and copolymers for lithium ion battery applications. *RSC Adv.*, ***3***, 11404–11417.
[42] **Lee, H., Yanilmaz, M., Toprakci, O., Fu, K., and Zhang, X.** (2014). A review of recent developments in membrane separators for rechargeable lithium-ion batteries. *Energy Environ. Sci.*, ***7***, 3857–3886.
[43] **Gao, K., Hu, X., Yi, T., and Dai, C.** (2006). PE-g-MMA polymer electrolyte membrane for lithium polymer battery. *Electrochimica Acta*, ***52***, 443–449.
[44] **Appetecchi, G.B., Croce, F., and Scrosati, B.** (1995). Kinetics and stability of the lithium electrode in poly(methylmethacrylate)-based gel electrolytes. *Electrochimica Acta*, ***40***, 991–997.
[45] **Bottino, A., Camera-Roda, G., Capannelli, G., and Munari, S.** (1991). The formation of microporous polyvinylidene difluoride membranes by phase separation. *Journal of Membrane Science*, ***57***, 1–20.
[46] **Djian, D., Alloin, F., Martinet, S., and Lignier, H.** (2009). Macroporous poly(vinylidene fluoride) membrane as a separator for lithium-ion batteries with high charge rate capacity. *Journal of Power Sources*, ***187***, 575–580.
[47] **Min, H.-S., Ko, J.-M., and Kim, D.-W.** (2003). Preparation and characterization of porous polyacrylonitrile membranes for lithium-ion polymer batteries. *Journal of Power Sources*, ***119–121***, 469–472.
[48] **Choi, B.K., Shin, K.H., and Kim, Y.W.** (1998). Lithium ion conduction in PEO–salt electrolytes gelled with PAN. *Solid State Ionics*, ***113–115***, 123–127.

[49] **Venugopal, G., Moore, J., Howard, J., and Pendalwar, S.** (1999). Characterization of microporous separators for lithium-ion batteries. *Journal of Power Sources*, ***77***, 34–41.

[50] **Li, X., Cheruvally, G., Kim, J.-K., Choi, J.-W., Ahn, J.-H., Kim, K.-W., et al.** (2007). Polymer electrolytes based on an electrospun poly(vinylidene fluoride-co-hexafluoropropylene) membrane for lithium batteries. *Journal of Power Sources*, ***167***, 491–498.

[51] **Manuel Stephan, A. and Saito, Y.** (2002). Ionic conductivity and diffusion coefficient studies of PVdF–HFP polymer electrolytes prepared using phase inversion technique. *Solid State Ionics*, ***148***, 475–481.

[52] **Abbrent, S., Plestil, J., Hlavata, D., Lindgren, J., Tegenfeldt, J., and Wendsjö, Å.** (2001). Crystallinity and morphology of PVdF–HFP-based gel electrolytes. *Polymer*, ***42***, 1407–1416.

[53] **Gozdz, A.S., Schmutz, C.N., and Tarascon, J.** (1994). Rechargeable lithium intercalation battery with hybrid polymeric electrolyte, 5296318, 1994.

[54] **Choi, S.W., Kim, J.R., Jo, S.M., Lee, W.S., and Kim, Y.-R.** (2005). Electrochemical and Spectroscopic Properties of Electrospun PAN-Based Fibrous Polymer Electrolytes. *J. Electrochem. Soc.*, ***152***, A989–A995.

[55] **Wu, Q.-Y., Liang, H.-Q., Gu, L., Yu, Y., Huang, Y.-Q., and Xu, Z.-K.** (2016). PVDF/PAN blend separators via thermally induced phase separation for lithium ion batteries. *Polymer*, ***107***, 54–60.

[56] **Raghavan, P., Zhao, X., Shin, C., Baek, D.-H., Choi, J.-W., Manuel, J., et al.** (2010). Preparation and electrochemical characterization of polymer electrolytes based on electrospun poly(vinylidene fluoride-co-hexafluoropropylene)/polyacrylonitrile blend/composite membranes for lithium batteries. *Journal of Power Sources*, ***195***, 6088–6094.

[57] **Ferrari, S., Nair, J.R., Zhou, Y., and Wan, C.** (2018). 10 - Polymer nanocomposites for lithium battery applications. in: M. Jawaid, M.M. Khan (Eds.), Polymer-Based Nanocomposites for Energy and Environmental Applications, Woodhead Publishing, pp. 283–313.

[58] **Wang, Q., Song, W.-L., Fan, L.-Z., and Song, Y.** (2015). Facile fabrication of polyacrylonitrile/alumina composite membranes based on triethylene glycol diacetate-2-propenoic acid butyl ester gel polymer electrolytes for high-voltage lithium-ion batteries. *Journal of Membrane Science*, ***486***, 21–28.

[59] **Gopalan, A.I., Santhosh, P., Manesh, K.M., Nho, J.H., Kim, S.H., Hwang, C.-G., et al.** (2008). Development of electrospun PVdF–PAN membrane-based polymer electrolytes for lithium batteries. *Journal of Membrane Science*, ***325***, 683–690.

[60] **Wu, D., Huang, S., Xu, Z., Xiao, Z., Shi, C., Zhao, J., et al.** (2015). Polyethylene terephthalate/poly (vinylidene fluoride) composite separator for Li-ion battery. *J. Phys. D: Appl. Phys.*, ***48***, 285305.

[61] **Huang, X.** (2011). Separator technologies for lithium-ion batteries. *J Solid State Electrochem*, ***15***, 649–662.

[62] **Arora, P. and Zhang, Z. (John)** (2004). Battery Separators. *Chem. Rev.*, ***104***, 4419–4462.

[63] **Deimede, V. and Elmasides, C.** (2015). Separators for Lithium-Ion Batteries: A Review on the Production Processes and Recent Developments. *Energy Technology*, ***3***, 453–468.

[64] **Lee, Y., Lee, H., Lee, T., Ryou, M.-H., and Lee, Y.M.** (2015). Synergistic thermal stabilization of ceramic/co-polyimide coated polypropylene separators for lithium-ion batteries. *Journal of Power Sources*, ***294***, 537–544.

[65] **An, M.-Y., Kim, H.-T., and Chang, D.-R.** (2014). Multilayered separator based on porous polyethylene layer, Al2O3 layer, and electro-spun PVdF nanofiber layer for lithium batteries. *J Solid State Electrochem*, ***18***, 1807–1814.

[66] **Zhang, F., Ma, X., Cao, C., Li, J., and Zhu, Y.** (2014). Poly(vinylidene fluoride)/SiO2 composite membranes prepared by electrospinning and their excellent properties for nonwoven separators for lithium-ion batteries. *Journal of Power Sources*, ***251***, 423–431.

[67] **Raghavan, P., Choi, J.-W., Ahn, J.-H., Cheruvally, G., Chauhan, G.S., Ahn, H.-J., et al.** (2008). Novel electrospun poly(vinylidene fluoride-co-hexafluoropropylene)–in situ SiO2 composite membrane-based polymer electrolyte for lithium batteries. *Journal of Power Sources*, ***184***, 437–443.

[68] **Guo, D., Sun, L., Zhang, X., Xiao, P., Liu, Y., and Tao, F.** (2018). The Causes of Fire and Explosion of Lithium Ion Battery for Energy Storage. in: 2018 2nd IEEE Conference on Energy Internet and Energy System Integration (EI2), pp. 1–5.

[69] **Wu, D., Shi, C., Huang, S., Qiu, X., Wang, H., Zhan, Z., et al.** (2015). Electrospun Nanofibers for Sandwiched Polyimide/Poly (vinylidene fluoride)/Polyimide Separators with the Thermal Shutdown Function. *Electrochimica Acta*, ***176***, 727–734.

[70] **Huang, H. and Wunder, S.L.** (2001). Preparation of microporous PVDF based polymer electrolytes. *Journal of Power Sources*, ***97–98***, 649–653.

[71] **Ding, Y., Zhang, P., Long, Z., Jiang, Y., Xu, F., and Di, W.** (2008). Preparation of PVdF-based electrospun membranes and their application as separators. *Sci. Technol. Adv. Mater.*, ***9***, 015005.

[72] **Lee, Y.-S., Jeong, Y.B., and Kim, D.-W.** (2010). Cycling performance of lithium-ion batteries assembled with a hybrid composite membrane prepared by an electrospinning method. *Journal of Power Sources*, ***195***, 6197–6201.

[73] **Jung, H.-R., Ju, D.-H., Lee, W.-J., Zhang, X., and Kotek, R.** (2009). Electrospun hydrophilic fumed silica/polyacrylonitrile nanofiber-based composite electrolyte membranes. *Electrochimica Acta*, ***54***, 3630–3637.

[74] **l'Abee, R., DaRosa, F., Armstrong, M.J., Hantel, M.M., and Mourzagh, D.** (2017). High temperature stable Li-ion battery separators based on polyetherimides with improved electrolyte compatibility. *Journal of Power Sources*, ***345***, 202–211.

[75] **Ansari, Y., Guo, B., Cho, J.H., Park, K., Song, J., Ellison, C.J., et al.** (2014). Low-Cost, Dendrite-Blocking Polymer-Sb2O3 Separators for Lithium and Sodium Batteries. *J. Electrochem. Soc.*, ***161***, A1655–A1661.

[76] **Zhao, Z., Li, J., Yuan, X., Li, X., Zhang, Y., and Sheng, J.** (2005). Preparation and properties of electrospun poly(vinylidene fluoride) membranes. *Journal of Applied Polymer Science*, ***97***, 466–474.

[77] **Wang, Y., Zhu, S., Sun, D., and Jin, Y.** (2016). Preparation and evaluation of a separator with an asymmetric structure for lithium-ion batteries. *RSC Adv.*, ***6***, 105461–105468.

[78] **Hwang, K., Kwon, B., and Byun, H.** (2011). Preparation of PVdF nanofiber membranes by electrospinning and their use as secondary battery separators. *Journal of Membrane Science*, ***378***, 111–116.

[79] **Liang, Y., Cheng, S., Zhao, J., Zhang, C., Sun, S., Zhou, N., et al.** (2013). Heat treatment of electrospun Polyvinylidene fluoride fibrous membrane separators for rechargeable lithium-ion batteries. *Journal of Power Sources*, ***240***, 204–211.

[80] **Kim, J.R., Choi, S.W., Jo, S.M., Lee, W.S., and Kim, B.C.** (2005). Characterization and Properties of P(VdF-HFP)-Based Fibrous Polymer Electrolyte Membrane Prepared by Electrospinning. *J. Electrochem. Soc.*, ***152***, A295–A300.

[81] **Kong, C.S., Yoo, W.S., Lee, K.Y., and Kim, H.S.** (2009). Nanofiber deposition by electroblowing of PVA (polyvinyl alcohol). *J Mater Sci*, ***44***, 1107–1112.

[82] **Demir, M.M., Yilgor, I., Yilgor, E., and Erman, B.** (2002). Electrospinning of polyurethane fibers. *Polymer*, ***43***, 3303–3309.

[83] **Wang, S., Zhao, X., Yin, X., Yu, J., and Ding, B.** (2016). Electret Polyvinylidene Fluoride Nanofibers Hybridized by Polytetrafluoroethylene Nanoparticles for High-Efficiency Air Filtration. *ACS Appl. Mater. Interfaces*, ***8***, 23985–23994.

[84] **Shi, L., Zhuang, X., Tao, X., Cheng, B., and Kang, W.** (2013). Solution blowing nylon 6 nanofiber mats for air filtration. *Fibers Polym*, ***14***, 1485–1490.

[85] **Park, H.-S. and Park, Y.O.** (2005). Filtration properties of electrospun ultrafine fiber webs. *Korean J. Chem. Eng.*, ***22***, 165–172.

[86] **Uppal, R., Bhat, G., Eash, C., and Akato, K.** (2013). Meltblown nanofiber media for enhanced quality factor. *Fibers Polym*, ***14***, 660–668.

[87] **Huang, Z.-X., Liu, X., Zhang, X., Wong, S.-C., Chase, G.G., Qu, J.-P., et al.** (2017). Electrospun polyvinylidene fluoride containing nanoscale graphite platelets as electret membrane and its application in air filtration under extreme environment. *Polymer*, ***131***, 143–150.

[88] **Zhang, S., Liu, H., Yin, X., Yu, J., and Ding, B.** (2016). Anti-deformed Polyacrylonitrile/Polysulfone Composite Membrane with Binary Structures for Effective Air Filtration. *ACS Appl. Mater. Interfaces*, ***8***, 8086–8095.

[89] **Zhang, S., Cao, J., Shang, Y., Wang, L., He, X., Li, J., et al.** (2015). Nanocomposite polymer membrane derived from nano TiO2-PMMA and glass fiber nonwoven: high thermal endurance and cycle stability in lithium ion battery applications. in: .

[90] **Prasanth, R., Shubha, N., Hng, H.H., and Srinivasan, M.** (2014). Effect of poly(ethylene oxide) on ionic conductivity and electrochemical properties of poly(vinylidenefluoride) based polymer gel electrolytes prepared by electrospinning for lithium ion batteries. *Journal of Power Sources*, ***245***, 283–291.

[91] **Yue, L., Zhang, J., Liu, Z., Kong, Q., Zhou, X., Xu, Q., et al.** (2014). A Heat Resistant and Flame-Retardant Polysulfonamide/Polypropylene Composite Nonwoven for High Performance Lithium Ion Battery Separator. *J. Electrochem. Soc.*, ***161***, A1032–A1038.

[92] **Hall, M.E., Zhang, J., and Horrocks, A.R.** (1994). The flammability of polyacrylonitrile and its copolymers III. Effect of flame retardants. *Fire and Materials*, ***18***, 231–241.

[93] **Chou, S. and Wu, C.-J.** (1995). Effect of Brominated Flame Retardants on the Properties of Acrylonitrile /Vinyl Acetate Copolymer Fibers. *Textile Research Journal*, ***65***, 533–539.

[94] **Zheng, W., Zhu, Y., Na, B., Lv, R., Liu, H., Li, W., et al.** (2017). Hybrid silica membranes with a polymer nanofiber skeleton and their application as lithium-ion battery separators. *Composites Science and Technology*, ***144***, 178–184.

CURRICULUM VITAE

Name Surname **: Adel Al Rai**

Place and Date of Birth **: 08.06.1992 Damascus**

E-Mail **: adelalrai@gamil.com**

EDUCATION **:**

- **B.Sc.** **:** 2015, University Of Sunderland, Faculty of Applied Sciences, Mechanical Engineering
- **M.Sc.** **:** 2019, Istanbul Technical University, Graduate School of Science and Technology, Material and Manufacturing

PROFESSIONAL EXPERIENCE AND REWARDS:

- 2018 – 2019 Research assistant, at Istanbul Technical University TEMAG Laboratory, Istanbul, Turkey
- 2017 – 2018 Project assistant, at Istanbul Technical University, Laboratory, Istanbul, Turkey
- 2015 – 2016 Web developer at UNIFY, United kingdom

PUBLICATIONS, PRESENTATIONS ON THE THESIS:

- **Rai, A.A., Stojanovska, E., Kilic, A., Safak, Y., Demir, A.** 2019. PVDFModacrylic-Based Nanofibrous Membrane as Separator for Battery Applications, *International Fiber and Polymer Research Symposium*, May 2-3, 2019 Istanbul, Turkey.
- **Rai, A.A., Stojanovska, E., Yetgin, E., Fidan, G., Kilic, A., Safak, Y., Demir, A.** 2019. Developing and Characterization of PVDF-Based Electret Filter Media, *International Fiber and Polymer Research Symposium*, May 2-3, 2019 Istanbul, Turkey.